A DYNAMICAL MODEL OF OROGRAPHIC RAINFALL

R. P. SARKER

Institute of Tropical Meteorology, Poona, India

ABSTRACT

A dynamical model for orographic rainfall with particular reference to the Western Ghats is presented. The model assumes a saturated atmosphere with pseudo-adiabatic lapse rate and is based on linearized equations. The rainfall, as computed from the theoretical model, is in good agreement, both in intensity and in distribution, with the observed rainfall on the windward side of the mountain. The model cannot explain the rainfall distribution on the lee side, which apparently is not due to the orography considered in the model.

A simple formula for rainfall intensity has also been found based on continuity of mass and continuity of moisture taking into account the convergence or divergence within a thin layer. Further modifications in the dynamical model are also suggested.

1. INTRODUCTION

The rainfall over the Western Ghats of India (fig. 1) during the southwest monsoon is often believed to be strongly orographic. But as yet there is no quantitative information as to the extent to which the orography of the Western Ghats plays a part in causing rainfall. However, the effect of topography is fairly well known in the sense that precipitation increases with altitude and is greater on the slopes facing the prevailing wind than on the lee slopes. The rainfall may occur from lifting of saturated air induced by other causes as well, viz., horizontal convergence and instability. As it is quite likely that rainfall due to orography, convergence, and instability may occur simultaneously in mountainous areas, it is worthwhile to examine the role played by orography in causing rainfall and its distribution.

In this paper, we shall examine the amount of orographic rainfall and its distribution along the orography with particular reference to the Western Ghats. As is well known, to explain the amount and distribution of orographic rainfall one has to consider the aspects of meteorology on three different scales. First, there are the large-scale synoptic factors which determine the characteristics of an air mass which crosses the hills, its wind speed and direction, its stability, and its humidity. This aspect has been studied by Douglas and Glasspoole [4]. Second, there is the microphysics of cloud and rain, which determines whether the water which is condensed as cloud will reach the ground as rain or snow, or whether it will be merely re-evaporated on the leeward side. This aspect received the attention of Ludlam [12], [13]. Third, and the most important, is the dynamics of air motion over and around the hill. This determines to what depth and through what extent the air mass at each level is lifted. This aspect was considered by Sawyer [20] for rainfall over the British Isles on the very highly simplified assumption that the air is lifted by orography at all levels and to the same extent. On this assumption, he computed rainfall and compared it with the observed rainfall averaged over the Welsh Mountains. An empirical model for computation of orographic precipitation is also available in a report of the U.S. Weather Bureau [26]. However, a sound dynamical model for orographic rainfall based on the theories of air flow over mountains is still lacking. We propose to give here a model for the orographic rainfall over the Western Ghats. This model gives the amount of rainfall due to lifting caused by orography and also accounts for the variation of rainfall along the slope.

2. THE DYNAMICAL MODEL

We consider below how far the moisture-laden air is lifted by the Western Ghats. In a previous paper the author [19] investigated the mountain wave phenomena over the Western Ghats and showed that the air mass during the winter months has sufficient stable stratification to produce lee waves. The air current near the Western Ghats during the southwest monsoon is substantially different. In this season, the air mass does not have that much stable stratification. It is more or less neutral for moist adiabatic processes or even sometimes unstable in some layers. The wind is westerly below and easterly aloft. Generally, the westerly wind increases from 10 kt. at the surface to about 30–40 kt. between 1 and 2 km. and then gradually decreases and becomes easterly at about 6–7 km. On a strong monsoon day, the westerly wind may extend up to 10 km. as well and also may be considerably stronger. Moreover, it has often a secondary maximum in the layer 5–6 km. The linearized perturbation equation is not quite suitable for such an air stream as the differential equation does have a singularity at the level where the westerly wind changes to easterly (i.e., $U=0$). However, confining our attention to low levels only (6–7 km.), we may still get a satis-

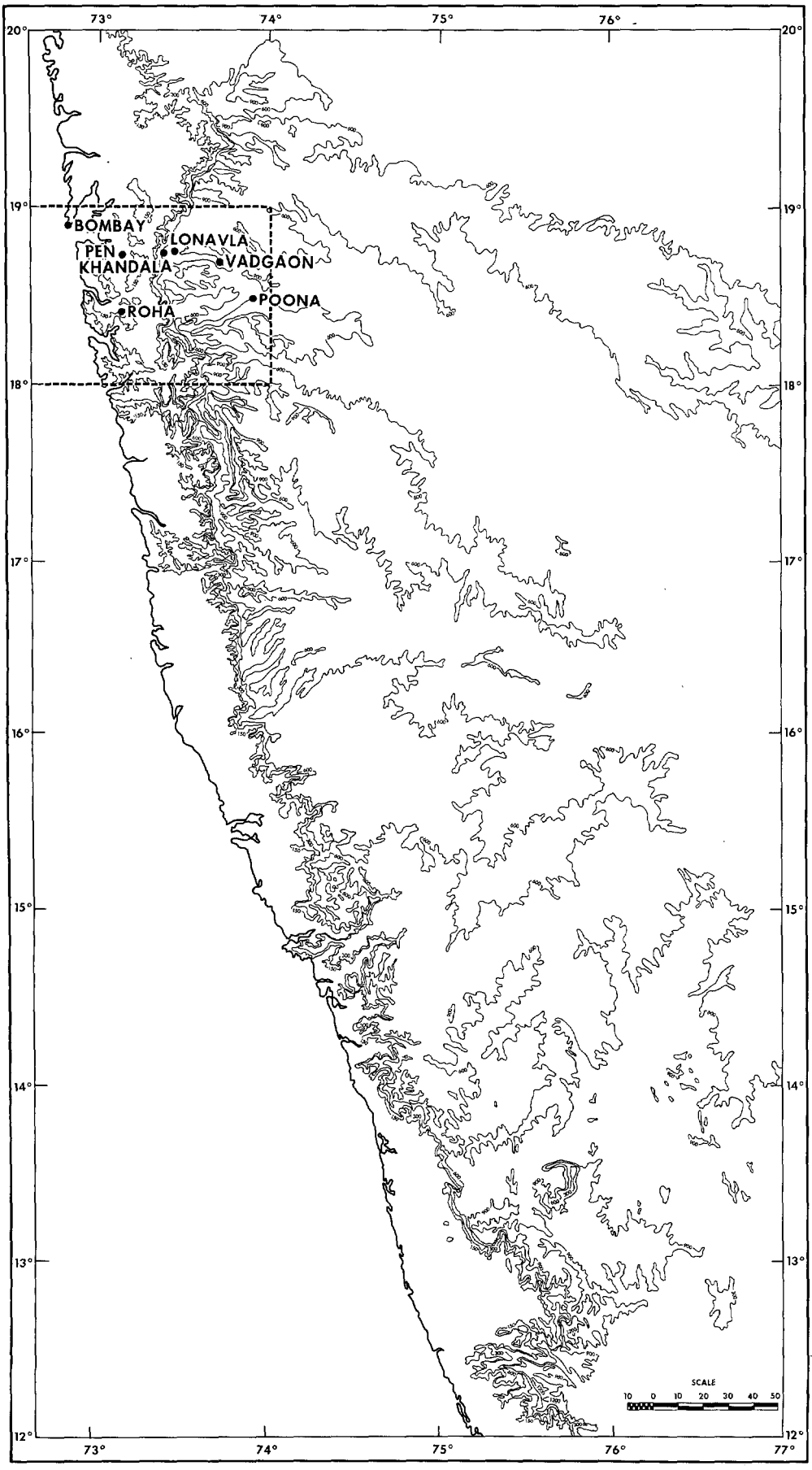

FIGURE 1.—Map of the Western Ghats. Contours are at 300-m. intervals above 300 m. The broken rectangle indicates the area under study. In the area, the open circles indicate locations of the rain-reporting stations. The x,z profile of the area within the rectangle is represented by equation (8).

factory approximate solution, as the motion within 6–7 km. is not much affected by the flow pattern above (Palm and Foldvik [17], Corby and Sawyer [1], and Sawyer [21]). We, therefore, base our dynamical model on the linearized equations.

We assume a two-dimensional flow in the vertical plane xz, with the z axis vertical and the x axis from west to east, i.e., in the direction of the undisturbed wind. In the two-dimensional flow the mountain is assumed to have an infinite extent in the y direction (south to north) and the flow is entirely over the mountain. This assumption is not far from reality as the Western Ghats extends for about 1500 km. in the S–N direction. We assume further (i) the undisturbed quantities are functions of z only, (ii) the perturbation quantities are small so that their product and higher-order terms are neglected compared to the undisturbed quantities, (iii) the motion is non-viscous and laminar, (iv) the earth's rotation is neglected, and (v) the motion is steady.

The basic equations are two equations of motion, equation of state, adiabatic equation, and equation of continuity. Starting with these equations and after linearization and elimination, we find the following differential equation for the vertical perturbation velocity (Sarker [19]):

$$\frac{\partial^2 W}{\partial z^2}+[f(z)-k^2]W=0 \tag{1}$$

where

$$f(z)=\frac{g(\gamma^*-\gamma)}{U^2T}-\frac{1}{U}\frac{d^2U}{dz^2}+\left(\frac{\gamma^*-\gamma}{T}-\frac{g}{\chi RT}\right)\frac{1}{U}\frac{dU}{dz}$$
$$-\frac{2}{\chi RT}\left(\frac{dU}{dz}\right)^2-\left(\frac{g-R\gamma}{2RT}\right)^2 \tag{2}$$

and the vertical velocity w is given by

$$w(x,z)=\mathrm{Re}\, W\cdot e^{ikx}\exp\left(\frac{g-R\gamma}{2RT}z\right)\simeq\mathrm{Re}\left(\frac{\rho_0}{\rho_z}\right)^{1/2}W\cdot e^{ikz} \tag{3}$$

In the above

U, T, ρ = undisturbed wind, temperature, and density respectively.
g = acceleration due to gravity.
γ^* = adiabatic lapse rate, dry or moist.
γ = actual lapse rate in the undisturbed atmosphere $= -dT/dz$.
R = gas constant.
$\chi = g/(g-R\gamma g\nu^*)$.
Re = Real part of( ).

The quantity χ becomes for a dry adiabatic lapse rate the ratio $c_p/c_v=1.4$ of specific heat at constant pressure to specific heat at constant volume. On the other hand for a moist adiabatic lapse rate, it varies with height.

Equation (1) gives the vertical velocity for a sinusoidal ground profile from which is obtained the vertical velocity for a smooth profile by the method of Fourier Integral.

The solution of equation (1) depends upon the behavior of $f(z)$ with z. We shall solve this equation for the condition during the monsoon. The monsoon air current is moist so that we assess the stability of the atmosphere relative to the saturated adiabatic lapse rate. We thus replace γ^* by γ_m the pseudo-adiabatic lapse rate. On examination of the actual lapse rate, it is seen that the atmosphere is more or less neutral or even sometimes slightly unstable as compared with the pseudo-adiabatic lapse rate. We, however, assume in our model a saturated atmosphere in which both the environment and the process have the pseudo-adiabatic lapse rate. Thus the atmosphere in our model has neutral stability and this is consistent with our assumption of laminar flow. The first term of the expression for $f(z)$ in (2) then vanishes and the second term, viz, the shear term, is the most important term as compared to the remaining three terms.

The variation of $f(z)$ with height can be seen in figures 3, 9, 12, 15, 19, 22. It is seen that $f(z)$ is positive in the lowest layer, it is negative in some middle layer corresponding to positive values of d^2U/dz^2, and again becomes positive above. We are, therefore, obliged to take in our model a negative value of $f(z)$ in the middle layer. We accordingly divide the atmosphere into three layers as follows:

$$\left.\begin{aligned} f(z)&=l_1^2 \text{ when } z\le z_0\\ &=-l_2^2 \qquad z_0\le z\le H\\ &=l_3^2 \qquad z\ge H\end{aligned}\right\} \tag{4}$$

The differential equation (1) for the three layers thus becomes:

Lowest Layer:

$$\frac{d^2W_1}{dz^2}+[l_1^2-k^2]W_1=0 \text{ for } z\le z_0 \tag{5}$$

Middle Layer:

$$\frac{d^2W_2}{dz^2}-[l_2^2+k^2]W_2=0 \text{ for } z_0\le z\le H \tag{6}$$

Upper Layer:

$$\frac{d^2W_3}{dz^2}+[l_3^2-k^2]W_3=0 \text{ for } z\ge H \tag{7}$$

3. SOLUTION FOR WESTERN GHATS

We now solve equations (5)–(7) for the Western Ghats profile. The location map of Western Ghats is shown in figure 1. The Ghats extends for about 1500 km. in the north–south direction. We have restricted our present investigation to the portion marked by the broken rectangle. For this area, the height on an average, rises from west to east gradually to 0.8 km. in a distance of 65 km. and then ends in a plateau of average height 0.6 km. The average west–east vertical cross section of this portion of the Ghats is shown schematically at the bottom

of figure 7 and suceeding rainfall rate graphs and can be represented by the equation

$$\zeta_s(x)=\frac{a^2b}{a^2+x^2}+a'\tan^{-1}\frac{x}{a}$$

$$=\int_0^\infty e^{-ak}\left(ab\cos kx+a'\frac{\sin kx}{k}\right)dk \qquad (8)$$

where $\zeta_s(x)$ is the elevation of the ground surface at the level $z=-h$ with the numerical values $h=0.25$ km., $a=18.0$ km., $b=0.52$ km., and $a'=(2/\pi)\times 0.35$ km. As mentioned earlier, we solve first equations (5)–(7) for a sinusoidal ground profile of wave number k and then generalize the solution for an arbitrary mountain by the method of Fourier Integral.

The solutions of equations (5)–(7) are

$$\left.\begin{aligned} W_1(z,k)&=E\cos\nu z+F\sin\nu z\\ W_2(z,k)&=C\cosh\mu z+D\sinh\mu z\\ W_3(z,k)&=Ae^{-\lambda z}+Be^{\lambda z}\end{aligned}\right\} \qquad (9)$$

where

$$\nu=\sqrt{l_1^2-k^2},\ \mu=\sqrt{k^2+l_2^2},\ \lambda=\sqrt{k^2-l_3^2} \qquad (9a)$$

The constants A, B, C, D, E, F are to be found from the boundary conditions.

At the upper boundary, we require that energy of the perturbation must remain finite at great heights, so that $W_3\to 0$ as $z\to\infty$. Also at the interfaces $z=z_0$ and $Z=H$ we require that both vertical velocity and pressure are continuous. These conditions require that W and dW/dz are continuous at the interfaces. Applying these conditions we have the following expressions for W_1, W_2, W_3:

$$\left.\begin{aligned} W_1(z,k)&=Ae^{-\lambda H}\left[\cos\nu(z-z_0)\left\{\cosh\mu(z_0-H)-\frac{\lambda}{\mu}\sinh\mu(z_0-H)\right\}+\frac{\mu}{\nu}\sin\nu(z-z_0)\left\{\sinh\mu(z_0-H)-\frac{\lambda}{\mu}\cosh\mu(z_0-H)\right\}\right]\\ W_2(z,k)&=Ae^{-\lambda H}\left[\cosh\mu(z-H)-\frac{\lambda}{\mu}\sinh\mu(z-H)\right]\\ W_3(z,k)&=Ae^{-\lambda z}\end{aligned}\right\} \qquad (10)$$

A is to be found from the lower boundary condition. At the lower boundary, we require the flow to be tangential to the surface. For the profile (8) this condition is $W_1(x,-h)=U(\zeta_s)\partial\zeta_s(x)/\partial x$ so that the linearized lower boundary condition is

$$W_1(x,-h)=U(-h)\frac{\partial}{\partial x}\int_0^\infty e^{-ak}\left(ab\cos kx+a'\frac{\sin kx}{k}\right)dk$$

$$=\mathrm{Re}\,U(-h)\frac{\partial}{\partial x}\int_0^\infty e^{-ak}\left(ab-i\frac{a'}{k}\right)e^{ikx}dk \qquad (11)$$

The solution satisfying this condition is

$$W_{1,2,3}(x,z)=\mathrm{Re}\,U(-h)\frac{\partial}{\partial x}\int_0^\infty e^{-ak}\left(ab-i\frac{a'}{k}\right)e^{ikx}\cdot\frac{\Delta_{1,2,3}(z,k)}{\Delta(k)}dk \qquad (12)$$

where

$$\Delta_1(z,k)=\cos\nu(z-z_0)\left\{\cosh\mu(z_0-H)-\frac{\lambda}{\mu}\sinh\mu(z_0-H)\right\}+\frac{\mu}{\nu}\sin\nu(z-z_0)\left\{\sinh\mu(z_0-H)-\frac{\lambda}{\mu}\cosh\mu(z_0-H)\right\}$$

$$\Delta_2(z,k)=\cosh\mu(z-H)-\frac{\lambda}{\mu}\sinh\mu(z-H)$$

$$\Delta_3(z,k)=e^{-\lambda(z-H)}$$

and

$$\Delta(k)=[\Delta_1(z,k)]_{z=-h}$$

$$=\cos\nu(h+z_0)\left\{\cosh\mu(z_0-H)-\frac{\lambda}{\mu}\sinh\mu(z_0-H)\right\}-\frac{\mu}{\nu}\sin\nu(h+z_0)\left\{\sinh\mu(z_0-H)-\frac{\lambda}{\mu}\cosh\mu(z_0-H)\right\}$$

Now, the value of the integral in (12) depends upon the behavior of the function of $\Delta(k)$ in the range of integration. If $\Delta(k)$ vanishes in the range of integration, then the integral becomes an improper integral. In that case, we define the value of the integral as the Cauchy principal value and we see that $W_{1,2,3}(x,z)$ can be adequately divided into two parts—the wave part and the forcing part. The wave part corresponds to the values of k where $\Delta(k)$ vanishes. However, in our present model we have seen that for all the cases studied here, there is no wave on the lee side of the mountain. It is seen that $\Delta(k)$ does not vanish for any real value of k and it increases very rapidly as k increases. The solution of (12) is thus only the forcing part. It is difficult to get an exact value of the integral in (12) and by following Scorer [22], [23] the approximate solution is obtained by putting $k=0$ in $[\Delta_{1,2,3}(z,k)]/\Delta(k)$. The approximation as Scorer recognizes, and as Sawyer [21] points out, is not good near the origin, but we are helped here to draw the streamlines as the flow is smooth. However, the vertical velocity as obtained from the approximate solution is not strictly representative of the actual vertical velocity in the neighborhood of $x=0$.

The approximate solution is

$$W_{1,2,3}(x,z)=\mathrm{Re}\,U(-h)\frac{\Delta_{1,2,3}(z,0)}{\Delta}\frac{\partial}{\partial x}\int_0^\infty e^{-ak}\left(ab-i\frac{a'}{k}\right)e^{ikx}dk$$

$$=\mathrm{Re}\,U(-h)\,\frac{\Delta_{1,2,3}(z,0)}{\Delta}\,\frac{\partial}{\partial x}\left[ab\,\frac{a+ix}{a^2+x^2}+a'\left\{\tan^{-1}\frac{x}{a}+\frac{i}{2}\ln\frac{a^2+x^2}{a^2}\right\}\right]\text{ for all } x \quad (13)$$

where Δ is the value of $\Delta(k)$ at $k=0$. When we put $k=0$, we get the following values of λ,μ,ν from (9a)

$$\lambda=\pm il_3,\ \mu=l_2,\ \nu=l_1 \quad (14)$$

There has been considerable controversy as to the choice of the sign of λ. Scorer in all his papers chose the positive sign. The rest of the workers in this field (viz., Corby and Sawyer [2], Palm [16], Queney et al. [18]) have shown that the negative sign for λ is the appropriate choice which places the lee waves downstream. This choice also has been confirmed by Crapper [3] by a rigorous analytical treatment. We have, accordingly, chosen the negative $\lambda=-il_3$ in (14). With this choice the values of $\Delta_{1,2,3}(z,0)$ and Δ in (13) are as follows:

$$\Delta=\cos l_1(h+z_0)\left\{\cosh l_2(z_0-H)+i\frac{l_3}{l_2}\sinh l_2(z_0-H)\right\}-\frac{l_2}{l_1}\sin l_1(h+z_0)\left\{\sinh l_2(z_0-H)+i\frac{l_3}{l_2}\cosh l_2(z_0-H)\right\}$$

$$\Delta_1(z,0)=\cos l_1(z-z_0)\left\{\cosh l_2(z_0-H)+i\frac{l_3}{l_2}\sinh l_2(z_0-H)\right\}+\frac{l_2}{l_1}\sin l_1(z-z_0)\left\{\sinh l_2(z_0-H)+i\frac{l_3}{l_2}\cosh l_2(z_0-H)\right\}$$

$$\Delta_2(z,0)=\cosh l_2(z-H)+i\frac{l_3}{l_2}\sinh l_2(z-H)$$

$$\Delta_3(z,0)=e^{il_3(z-H)} \quad (15)$$

Expression (13), with the values of $\Delta_{1,2,3}(z,0),\Delta$ in (15), when multiplied by $(\rho_s/\rho_z)^{1/2}$ gives the vertical velocity due to the mountain. The corresponding displacement $\zeta_s(x,z)$ of the streamline above its original undisturbed level z is given by

$$\zeta_{1,2,3}(x,z)=\frac{1}{U}\int W_{1,2,3}(x,z)\,dx$$

$$=\mathrm{Re}\left(\frac{\rho_s}{\rho_z}\right)^{1/2}\frac{U(-h)}{U(z)}\cdot\frac{\Delta_{1,2,3}(z,0)}{\Delta}\cdot\left[ab\,\frac{a+ix}{a^2+x^2}+a'\left\{\tan^{-1}\frac{x}{a}+\frac{i}{2}\ln\frac{a^2+x^2}{a^2}\right\}\right] \quad (16)$$

In the above ρ_s is the undisturbed density of air at the ground and ρ_z is the density at a level z above the origin.

227-347 O—66——3

4. COMPUTATION OF RAINFALL

We now make use of the vertical velocity obtained from our dynamical model to compute rainfall and its spatial distribution along the orography of the Western Ghats (fig. 1).

As mentioned earlier, we assume a saturated atmosphere. Rainfall for pseudo-adiabatically ascending air has been computed by many authors; viz., Fulks [5], Showalter [24], Kuhn [9], and Thompson and Collins [25]. Fulks and Showalter both assume that there is no divergence at the bottom and the top of a layer. As will be seen from the vertical velocity profiles to be presented, this assumption is not true in our case. While Thompson and Collins take initial unsaturated conditions into account, Kuhn takes into account the divergence or convergence at the bottom and top of a layer. However, it appeared to the author that in all the above formulas, the continuity of mass of air within the layer has been ignored. We accordingly derive below a formula for rainfall computation based on simple physical considerations so as to take into account the continuity of mass also.

Let Δz be the thickness of a column of air of unit cross section. If ρ_0,ρ_1 be the density of dry air at the bottom and top of the layer and W_0,W_1 be the corresponding vertical velocities, then the mass of air entering at the bottom of the layer is ρ_0W_0 and the mass leaving the top is ρ_1W_1. Now if $\rho_0W_0\neq\rho_1W_1$ there is either divergence or convergence (two dimensional) in the layer. If $\rho_0W_0>\rho_1W_1$ there is divergence so that the mass of air that leaves the column sideways is $\rho_0W_0-\rho_1W_1$ and considering that the thickness of air column is small, we can with sufficient accuracy assume that the mass leaves the column sideways at its middle point. Thus if x_0, x_1 be the humidity mixing ratios of saturated air at the bottom and top of the layer, and x' that at the middle, the quantity of moisture that enters the column is $\rho_0W_0x_0$ and the quantity that leaves is $[\rho_1W_1x_1+(\rho_0W_0-\rho_1W_1)x']$. Thus, assuming that the rate of precipitation is equal to the rate of condensation, we find that the amount of rainfall from the column is

$$[\rho_0W_0x_0-\{\rho_1W_1x_1+(\rho_0W_0-\rho_1W_1)x'\}]$$

expressed in proper units. If density is expressed as kgm.$^{-3}$, humidity mixing ratio as gm. kgm.$^{-1}$ and vertical velocity as cm. sec.$^{-1}$, then the rainfall intensity is

$$I=0.036[\rho_0W_0x_0-\{\rho_1W_1x_1+(\rho_0W_0-\rho_1W_1)x'\}]\text{ mm./hr.}$$
$$=0.036[\rho_0W_0(x_0-x')+\rho_1W_1(x'-x_1)]\text{mm./hr.} \quad (17)$$

As a very good approximation we could replace x' by the mean value $(x_0+x_1)/2$ of the column. Formula (17) is also the expression for rainfall intensity when there is convergence in the layer, that is, when $\rho_1W_1>\rho_0W_0$. The above simple formula is believed to be an improvement upon the existing formulas for computation of rainfall intensity, as it considers, apart from continuity of moisture, the continuity of mass also when there is divergence or convergence within a layer. We have

applied this formula to compute rainfall intensity for 500-m. thicknesses from surface to 6–7 km. up to which our dynamical model for vertical velocity is believed to be valid.

DOWNWIND EXTENSION OF PRECIPITATION

The rain that falls from a particular layer will not necessarily fall vertically below the layer, for the airstream will carry it downstream. Any realistic model for space distribution of precipitation must take this into account. This effect on the appearance of precipitation patterns on a radar screen and on the size dispersion of raindrops has been discussed by Marshall [14], Langleben [10], Gunn and Marshall [7] and Mason and Andrews [15]. Their discussions have dealt mainly with the generating cells moving with the wind velocity at the level of the generating cell. We consider below the horizontal extension of the precipitation along the wind in the case of fixed generating cells.

If $U(z)$ be the horizontal wind at the level z and p be the terminal velocity of the precipitation element (which is a snow flake above the freezing level and a melted droplet below the freezing level), then the horizontal distance x traveled by the precipitation element created at an anchored generating cell at the level z_0 in falling to the level z is given by

$$x=\frac{1}{p}\int_z^{z_0} U(z)dz \tag{18}$$

The above formula is derived on the two assumptions that (i) the rate of descent of the precipitation element is constant and is equal to its terminal velocity, and (ii) the precipitation element moves horizontally with the speed of the wind. The integral in (18) is equivalent to the area bounded by the graph of $U(z)$ against z, the z-axis and the levels z_0 and z.

TERMINAL VELOCITY OF PRECIPITATION ELEMENTS

We have assumed a pseudo-adiabatic condition in our model which places the freezing level at a particular height. This level generally lies at 5.5 km. This may, of course, vary from one case to another. The precipitation element above the freezing level is a snow flake and a melted droplet below. The terminal velocities accordingly are different above and below the freezing level. The orographic rainfall, as will be seen later, generally varies from 2–8 mm./hr. According to Kelkar [8] the most probable drop-diameter corresponding to this rate of precipitation is 1.00–1.25 mm. The terminal velocity corresponding to this drop-diameter is 4.5 m. sec.$^{-1}$ (Gunn and Kinzer [6], reproduced by List [11]) in the liquid phase and 1.00 m. sec.$^{-1}$ in the snow phase (Langleben [10]).

Using these terminal velocities and the given wind profile we construct the trajectory which a precipitation element starting at a particular level will follow to reach the ground.

5. NUMERICAL COMPUTATION

We have performed numerical computations for seven cases when the monsoon was strong as well as weak. We have taken both individual days as well as a few spells of 3 to 4 days. For the undisturbed wind and temperature we have taken data of Santacruz (19°07′ N., 72°51′ E.) which is a sea level station on the windward side of the Western Ghats at a distance of 65 km. from the crest. For temperature we have, of course, taken the pseudo-adiabatic line through the surface dew point, or surface dry bulb, or mean in order to be realistic in regard to the actual distribution of temperature and dew point. The wind and temperature distributions are given in figures 2, 8, 11, 14, 18, 21 and those of $f(z)$ in figures 3, 9, 12, 15, 19, 22. The continuous line for $f(z)$ shows its actual distribution and the dashed lines show the

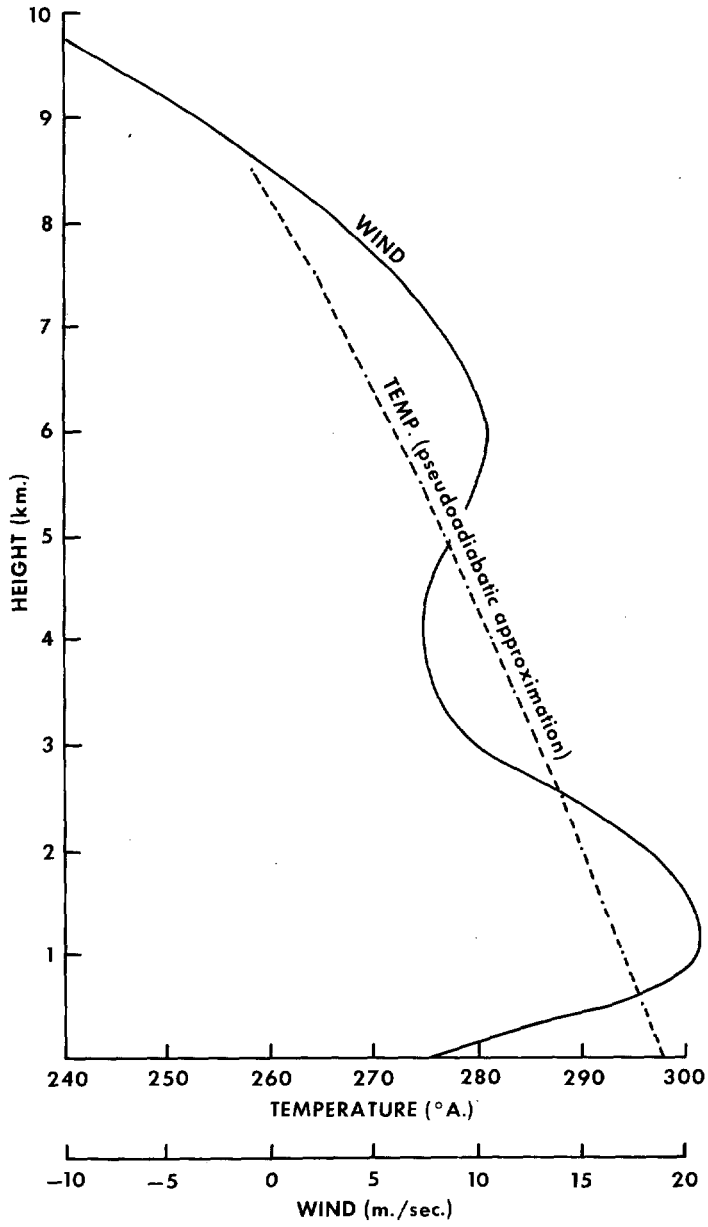

FIGURE 2.—Average wind and temperature profiles for July 5, 1961 (case I). Positive wind is westerly, negative is easterly.

TABLE 1.—*Constant values taken for $f(z)$ for the different layers, and boundary heights of the layers, for the cases studied*

Case No.	Date	Top of first layer z_0+h (km.)	Top of middle layer $H+h$ (km.)	l_1^2 km.$^{-2}$ value of $f(z)$ in first layer	l_2^2 km.$^{-2}$ value of $f(z)$ in middle layer	l_3^2 km.$^{-2}$ value of $f(z)$ in upper layer
I	July 5, 1961	2.50	5.00	0.36	−0.25	0.16
II	June 25, 1961	3.25	5.25	0.25	−0.15	0.25
III	July 6–9, 1963	1.75	3.25	0.60	−0.15	0.16
IV	July 11–12, 1958	2.50	4.00	0.36	−0.10	0.16
V	July 21, 1959	2.50	4.00	0.30	−0.16	0.13
VI	July 2–4, 1960	2.00	4.00	0.45	−0.075	0.075
VII	July 4–6, 1958	2.25	----------	0.49	----------	0.16

constant values taken for $f(z)$ at the different levels. The values of the parameters l_1^2, l_2^2, l_3^2, and z_0+h, $H+h$ are given in table 1. We now discuss the different cases.

CASE I—JULY 5, 1961

In figure 2 is given the relevent undisturbed wind and temperature distribution for Case I, July 5, 1961. The surface wind is 8 m./sec. The maximum wind is 20.5 m./sec. at a level 1–1.5 km. The wind then decreases to 7.5 m./sec. at 4 km., and again increases to 10.5 m./sec. at 6 km., then decreases and becomes easterly at 8.5 km. The surface temperature is 300° A. and the surface dew point is 298° A. In the model, we have assumed for temperature the pseudo-adiabatic line through the surface dew point 298° A. The relative humidity available up to 4.3 km. (600 mb.) varies from 80 to 100 percent.

The distribution of the function $f(z)$ with z is shown in figure 3, and the values of dU/dz and d^2U/dz^2 are given in figure 4. d^2U/dz^2 is negative from surface to 2.5 km. It is then positive up to 5 km. and is then again negative. The function $f(z)$ is positive up to 2.5 km., is negative in the layer 2.5 to 5.0 km., and is then positive. Accordingly, as mentioned earlier, we have divided the atmosphere into three layers. The layer surface to 2.5 km. has the constant value 0.36 km.$^{-2}$ for $f(z)$, the layer 2.5–5 km. has the constant value −0.25 km.$^{-2}$, and the upper layer has the constant value 0.16 km.$^{-2}$ This last value was chosen to represent $f(z)$ in the entire upper atmosphere, as this will not affect the motion below. The streamlines for this case are given in figure 5. It is seen that the crest of the streamlines tilts upstream. The motion descends beyond the top of the mountain. Descending motion

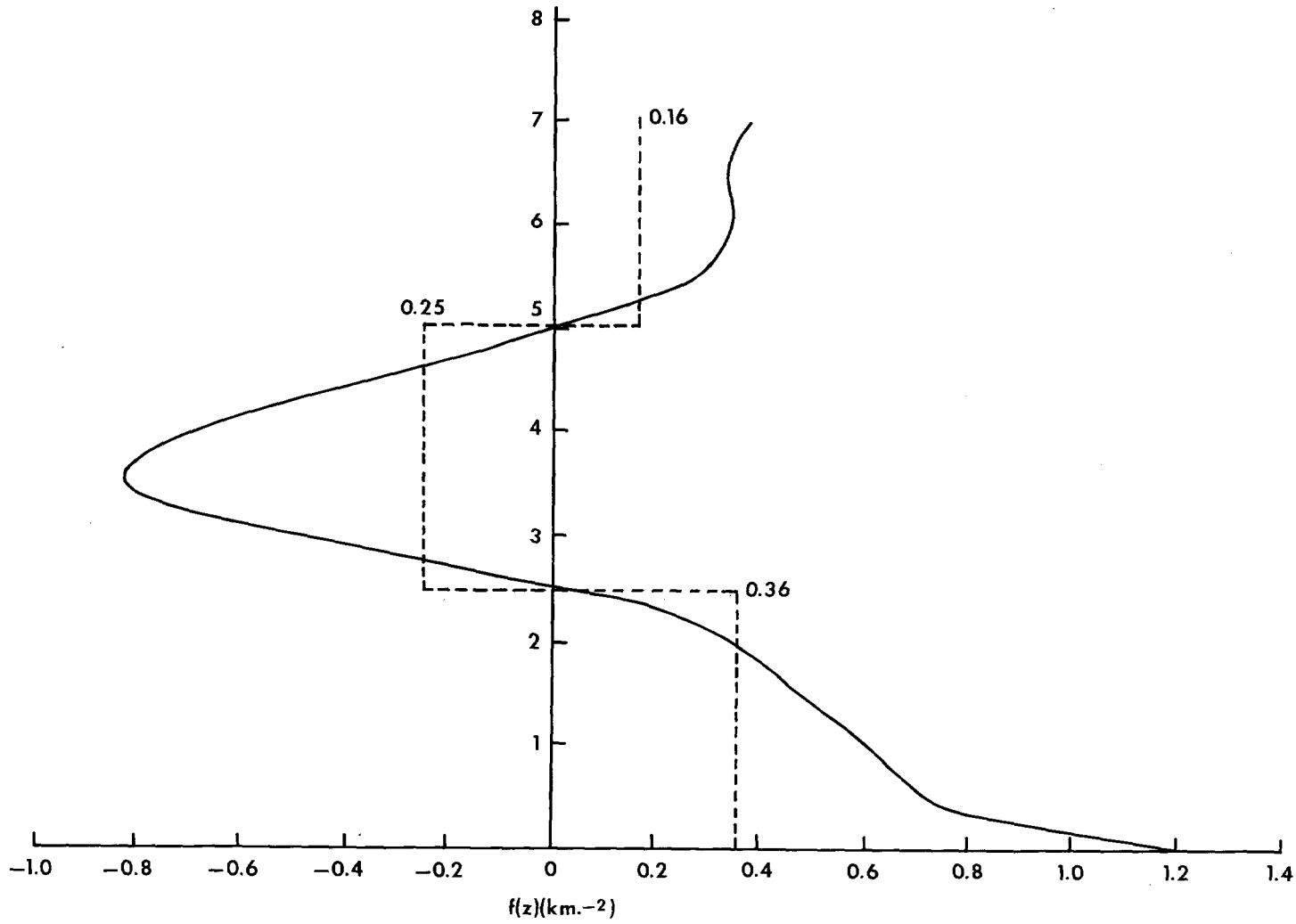

FIGURE 3.—Profile of $f(z)$ for July 5, 1961 (case I).

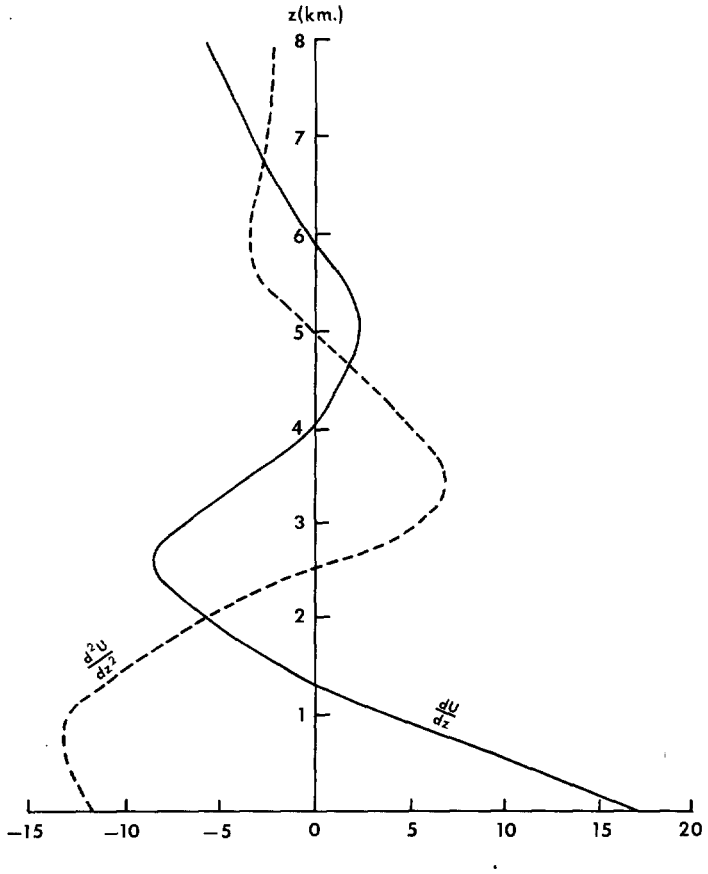

FIGURE 4.—Profiles of dU/dz (m.sec.$^{-1}$ km.$^{-1}$) and d^2U/dz^2 (m.sec.$^{-1}$ km.$^{-2}$) for July 5, 1961 (case I).

starts even earlier in the upper level. The distribution of the perturbation vertical velocity with height z and horizontal distance x is depicted in figures 6 (a), (b).

The ascending motion starts before the mountain is reached and the magnitude in general increases as one proceeds along the mountain toward the peak. This continues up to $x=-5$ km., i.e., 10 km. from the crest. The magnitude then decreases till $x=3$, i.e., 2 km. from the crest, after which ascending motion is replaced by descending motion. Also we see that in general, vertical velocity first increases with height and then decreases and then becomes negative; that is, an ascending motion below is replaced by descending motion above. Also the level of non-divergence, i.e., maximum vertical velocity, gradually decreases as we proceed from the coast toward the crest of the mountain. The variation of vertical velocity along the direction x itself suggests that rainfall along the orography cannot be uniform.

The rainfall distribution along the orography is given in figure 7. The solid line shows the observed intensity and the dashed line represents the orographic intensity as obtained by our model. For observed rainfall we have taken the section 20 mi. north-south of the Bombay-Poona region and for this section the only stations available are: Bombay at the coast; Pen and Roha about 20-25 km. from the coast; Khandala and Lonavla at 13 and 10 km. on the windward side from the crest, respectively; and

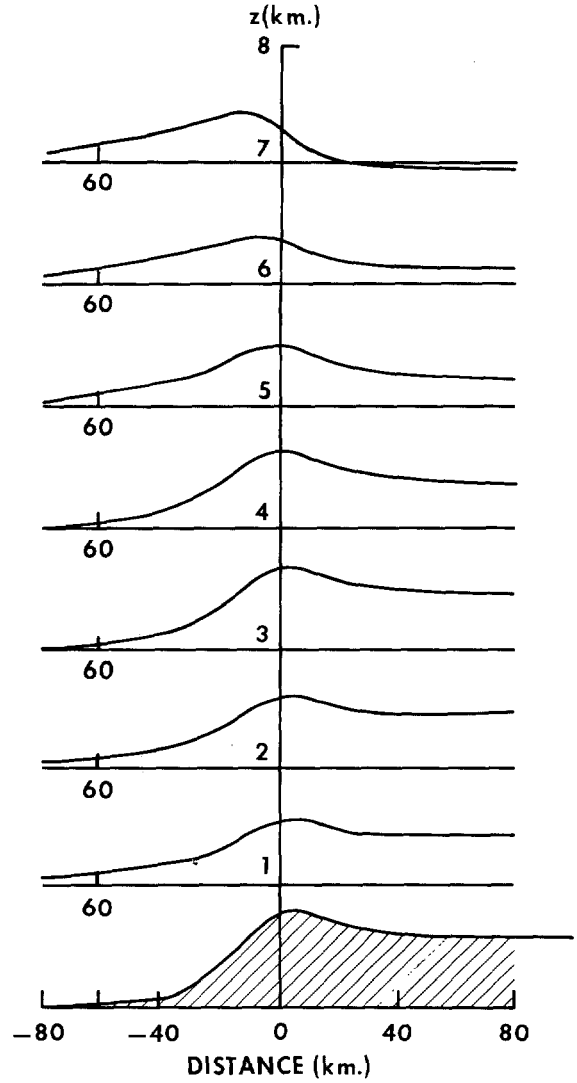

FIGURE 5.—Streamline displacements set up by the mountain on July 5, 1961 (case I).

Vadgaon and Poona on the lee-side plateau at distances of 5 and 40 km. from the crest (see fig. 1).

In figure 7, the theoretically computed orographic rainfall at the coast is 1.2 mm./hr. where the actual rainfall is 6.2 mm./hr. The highest computed orographic rainfall is 8.4 mm./hr. and the highest observed rainfall is 12.2 mm./hr. There is very close agreement between the positions of the peaks of the observed and the theoretically computed rainfall. Both the observed and orographic rainfall fall sharply beyond the peak rainfall. At the top of the mountain the theoretically computed rainfall is 2 mm./hr. and the observed value is 4 mm./hr. Beyond this the computed orographic rainfall is little and is nil beyond 10 km. from the crest. The observed peak is at a distance of 10 km. from the crest and the theoretically computed peak is 12 km. from the crest. The theoretically computed peak value is 69 percent of the observed peak.

CASE II—JUNE 25, 1961

For Case II, June 25, 1962 the relevant average wind

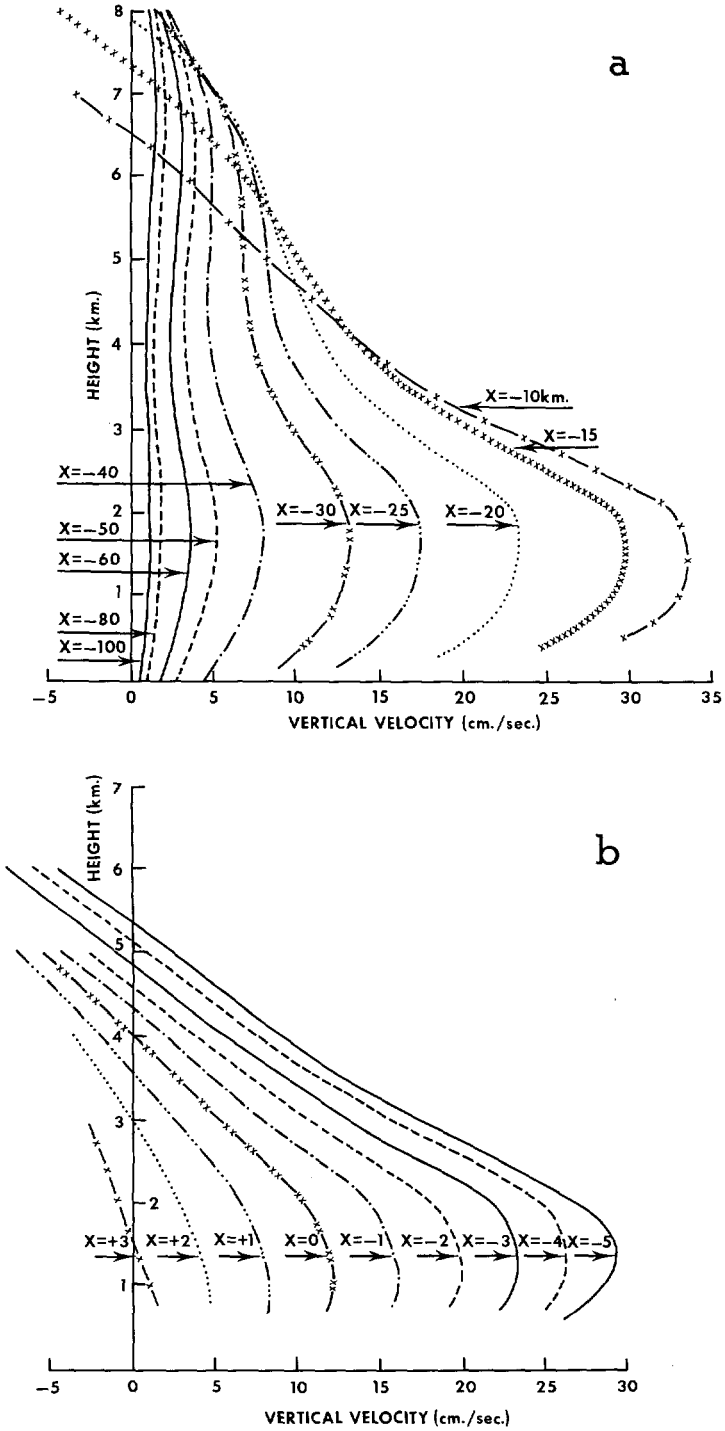

FIGURE 6.—Perturbation vertical velocity W (cm./sec.) profiles at different distances x along the orography on July 5, 1961 (case I). $x=5$ is the crest of the mountain. (a) Profiles for -100 km. $\leq x \leq -10$ km., $x=-60$ is the coastal position; $x=-80$, -100 are points at sea. (b) Profiles for -5 km. $\leq x \leq +3$ km.

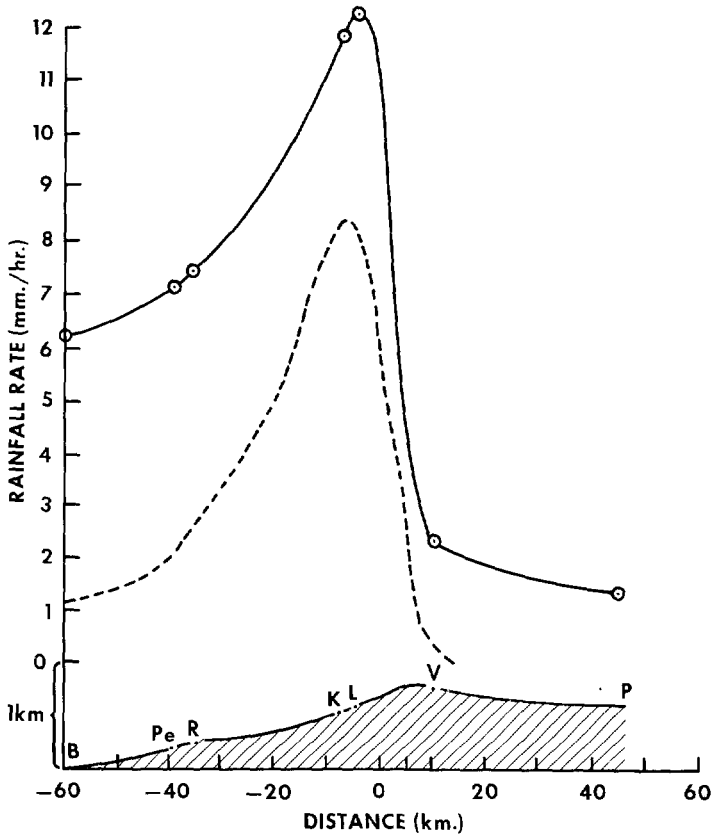

FIGURE 7.—Observed (upper solid curve) and theoretically computed (dashed curve) rainfall distribution for July 5, 1961 (case I) along the orographic profile (lower solid curve) from the coast at Bombay (B), inland through Pen (Pe), Roha (R), Khandala (K), Lonavla (L), Vadgaon (V), and Poona (P).

and temperature data are given in figure 8. The wind increases from 6.5 m./sec. at surface to 25 m./sec. at 2 km. It then decreases to 15 m./sec. at 4.5 km., again increases to 20 m./sec. at 6 km., and then decreases to 11 m./sec. at 7.5 km. above which data are not available. The surface dry bulb temperature, is 300° A. and the dew point is 298° A. In the model, we have chosen the pseudo-adiabatic line through 299° A. The relative humidity varies from 80 to 90 percent within 600 mb. (4.4 km.). The $f(z)$ profile (fig. 9) has been represented by three layers, viz., 0.25 km.$^{-2}$ up to 3.25 km., -0.15 km.$^{-2}$ up to 5.25 km., and then 0.25 km.$^{-2}$ above. The streamlines are of similar nature to the first case. The motion descends at all levels beyond the crest of the mountain. Ascending motion starts before the mountain is reached and it increases as we move along the orography till $x=-5$ km. (i.e., 10 km. from the crest) after which it gradually decreases and beyond $x=3$ km. the motion descends. Also the vertical velocity first increases with height, then decreases, and then becomes negative.

The observed and theoretically computed rainfall distribution are given in figure 10. The computed rainfall distribution follows the same pattern as the actual distribution up to the peak of the mountain. The computed rainfall at the coast is 1.2 mm./hr. and the observed intensity is 2.0 mm./hr., i.e., the orographic rainfall at the coast is 60 percent of the observed rainfall. Up to the peak rainfall the computed rainfall falls short by 0.6 to 1.0 mm./hr. of the observed rainfall. The maximum observed rainfall is 8.6 mm./hr. The computed orographic maximum is 7.7 mm./hr. or 90 percent of the actual. Also there is close agreement between the positions of the peaks. They differ by only 2 km. Rainfall

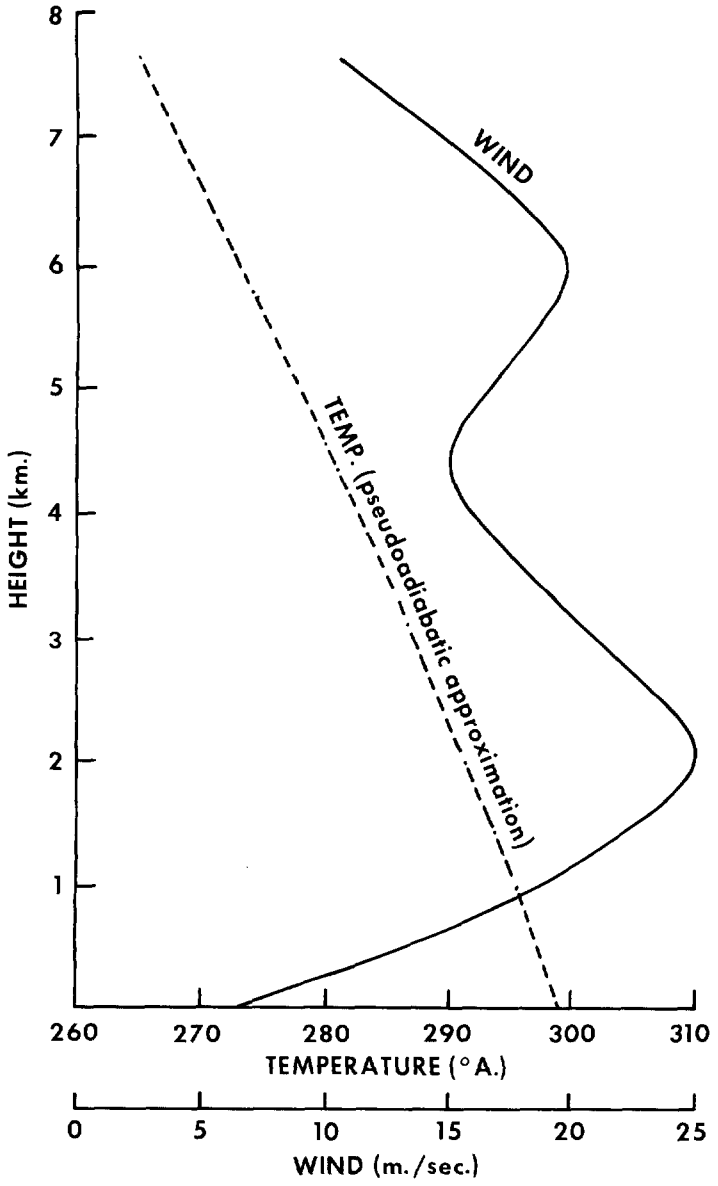

FIGURE 8.—Average wind and temperature profiles for June 25, 1961 (case II).

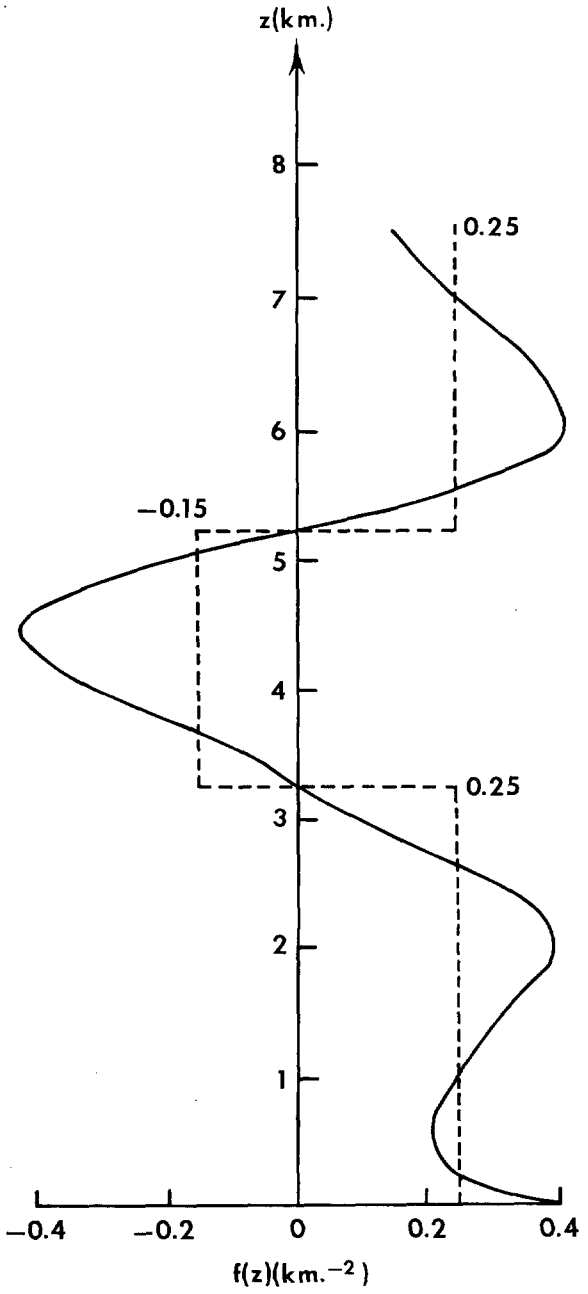

FIGURE 9.—Profile of $f(z)$ for June 25, 1961 (case II).

(observed as well as computed orographic) falls off sharply beyond the peak. At the top of the mountain rainfall (computed orographic as well as observed) is 3 mm./hr. The computed rainfall is nil beyond 15 km. from the top. Moreover, the rainfall beyond the crest results only from spillover as there is no ascending motion beyond the top.

CASE III—JULY 6–9, 1963

For Case III, the rainfall spell of July 6–9, 1963, the average wind and temperature distributions are given in figure 11, which is based on the data of July 5 (1730 IST) to July 8 (1730 IST). We have ensured that the processes during this period were more or less constant. The wind speed increases from 6 m./sec. at the surface to 15.5 m./sec. at 1 km. It then decreases to 11 m./sec. at 2.5 km., again slowly rises to 12 m./sec. at 4 km., and then decreases to 2 m./sec. at 7 km. The surface temperature is 298° A. and the dew point 297° A. We have taken the pseudo-adiabat through 297° A. The relative humidity varies from 90 to 100 percent up to 600 mb. (4.3 km.). The $f(z)$ profile (fig. 12) is negative in the layer 1.75 to 3.25 km. corresponding to positive values of d^2U/dz^2. The constant values taken for $f(z)$ are 0.60 km.$^{-2}$ up to 1.75 km., −0.15 km.$^{-2}$ up to 3.25 km., and 0.16 km.$^{-2}$ above 3.25 km. The streamline and vertical velocity profiles have the same pattern as in the first case. However the descending motion starts earlier. Ascending motion starts well before the mountain is reached. It increases and then begins to decrease from 15 km. from the peak. Beyond $x=1$ km. the motion descends at all levels.

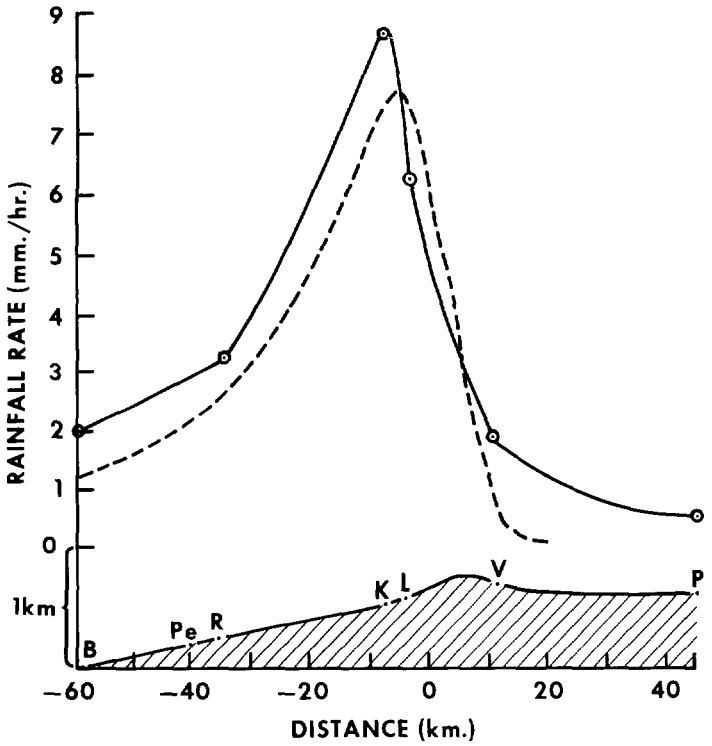

FIGURE 10.—Rainfall distribution for June 25, 1961 (case II). See legend for figure 7.

In figure 13, the computed orographic rainfall is 1.4 mm./hr. at the coast and the observed rainfall is 2.4 mm./hr., that is, the orographic rainfall is 60 percent of the observed value. The maximum rainfall is 7.8 mm./hr. and the computed maximum orographic rainfall is 5.9 mm./hr., i.e., 76 percent of the observed rainfall. The computed orographic peak occurs 14 km. from the top of the mountain and the observed peak, 10 km. Both the rainfall curves fall sharply beyond their peak. The computed orographic rainfall at the top of the mountain is nil, whereas the actual rainfall is 2.8 mm./hr. In this case there is no spillover, for, in the model, the ascending motion stops about 4 km. before the top is reached.

CASE IV—JULY 11–12, 1965

The relevant data of wind and temperature are given in figure 14 for Case IV, the rainfall spell of July 11–12, 1965. The wind speed increases from 8 m./sec. at the surface to 18.5 m./sec. at 2.0 km. It then decreases to 15 m./sec. at 3.5 km., rises to 16 m./sec. at 4.5 km., and then decreases and becomes easterly at 8.5 km. The surface dry bulb temperature is 299° A. and the dew point is 298° A. We have taken the pseudo-adiabatic line through 298° A. The relative humidity varies from 85 to 100 percent. The $f(z)$ profile (fig. 15) is negative in the layer 2.5 to 4.0 km. corresponding to positive values of d^2U/dz^2. The constant values of $f(z)$ chosen are 0.36 km.$^{-2}$ up to 2.50 km., -0.10 km.$^{-2}$ up to 4.0 km., and 0.16 km.$^{-2}$ above. The streamline and vertical velocity distributions have patterns similar to the other cases.

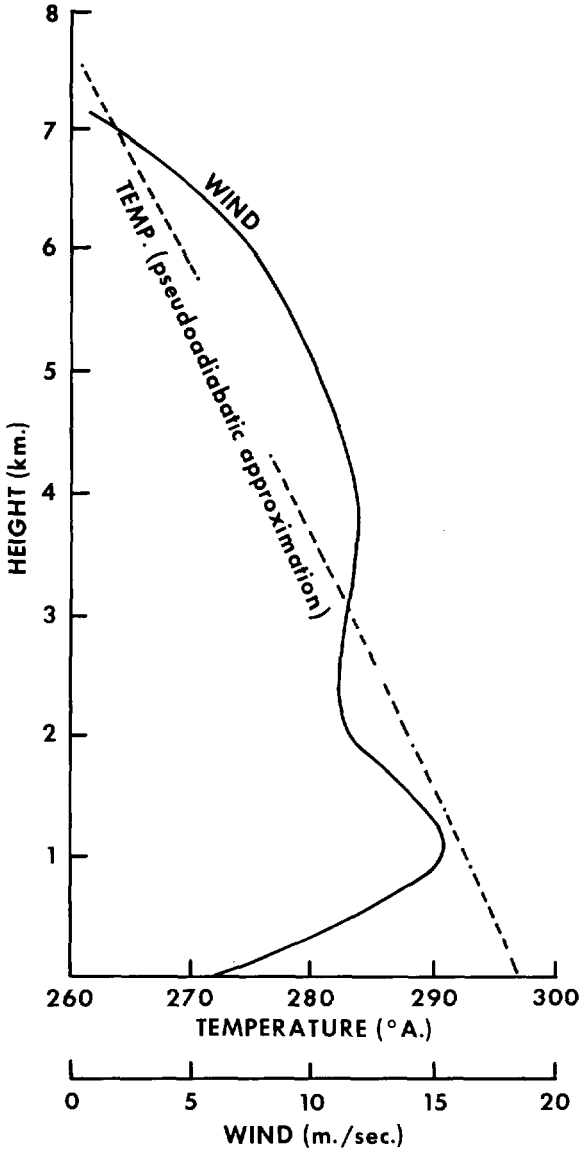

FIGURE 11.—Average wind and temperature profiles for July 6–9, 1963 (case III).

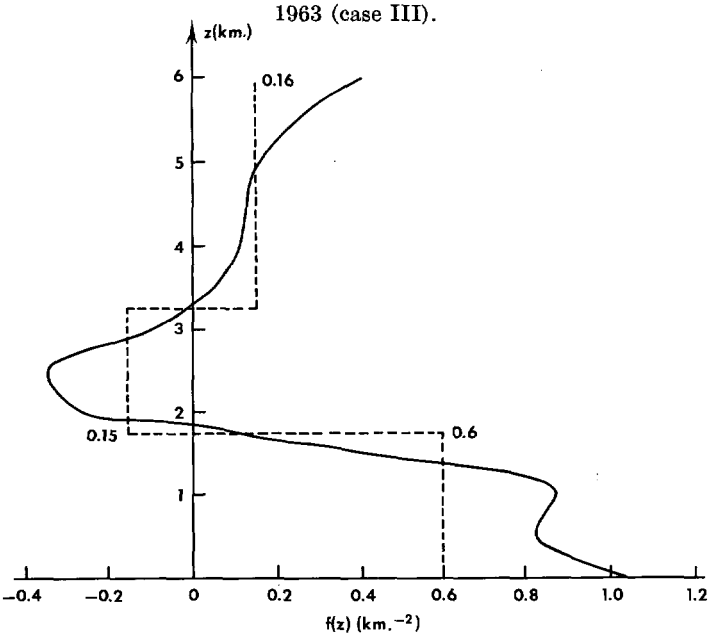

FIGURE 12.—Profile of $f(z)$ for July 6–9, 1963 (case III).

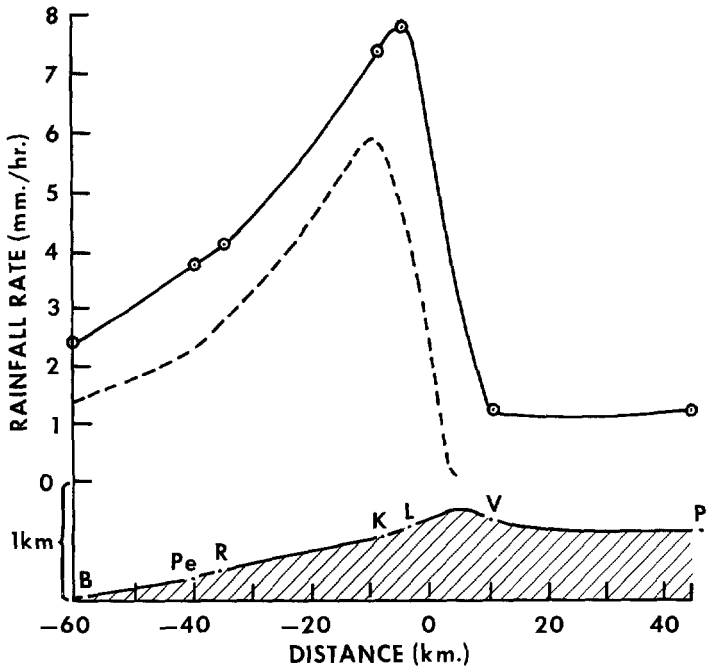

FIGURE 13.—Rainfall distribution for July 6–9, 1963 (case III). See legend for figure 7.

As usual, the ascending motion starts well before the mountain is reached. It increases, then decreases, and beyond $x=0$, i.e., 5 km. from the top, the motion is descending. Along the vertical it first increases, then decreases, and then becomes negative.

Both the computed orographic and the observed rainfall (fig. 16) at the coast are 2.2 mm./hr. This time the entire rainfall from the coast to the position of rainfall peak seems to be due to orography. However, the computed maximum orographic rainfall (8.8 mm./hr.) falls short of the observed peak rainfall by 1.0 mm./hr. The computed orographic peak value is thus 90 percent of the observed peak value. Also the computed orographic peak occurs 3 km. before the observed peak. The computed orographic rainfall falls off very sharply beyond its peak, whereas the fall of observed rainfall is not so sudden. The computed orographic rainfall at the crest is nil, whereas the observed value is near 5 mm./hr. The spillover effect is nil as descending motion starts from 5 km. before the top is reached.

CASE V—JULY 21, 1959

The relevant wind and temperature data for Case V, July 21, 1959, (not illustrated) show that the wind speed increases from 9 m./sec. at the surface to 16 m./sec. at 2 km. It then decreases to 11 m./sec. at 3.5 km. The wind then again increases with a secondary maximum of 12 m./sec. at 4.5 km. after which it decreases and gradually becomes easterly at 8.5 km. The surface dry bulb temperature is 299° A. and the dew point is 298° A. In the model we have taken the pseudoadiabat through 298° A. The relative humidity values available vary in the range 85 to 95 percent. The $f(z)$ profile is negative in the layer

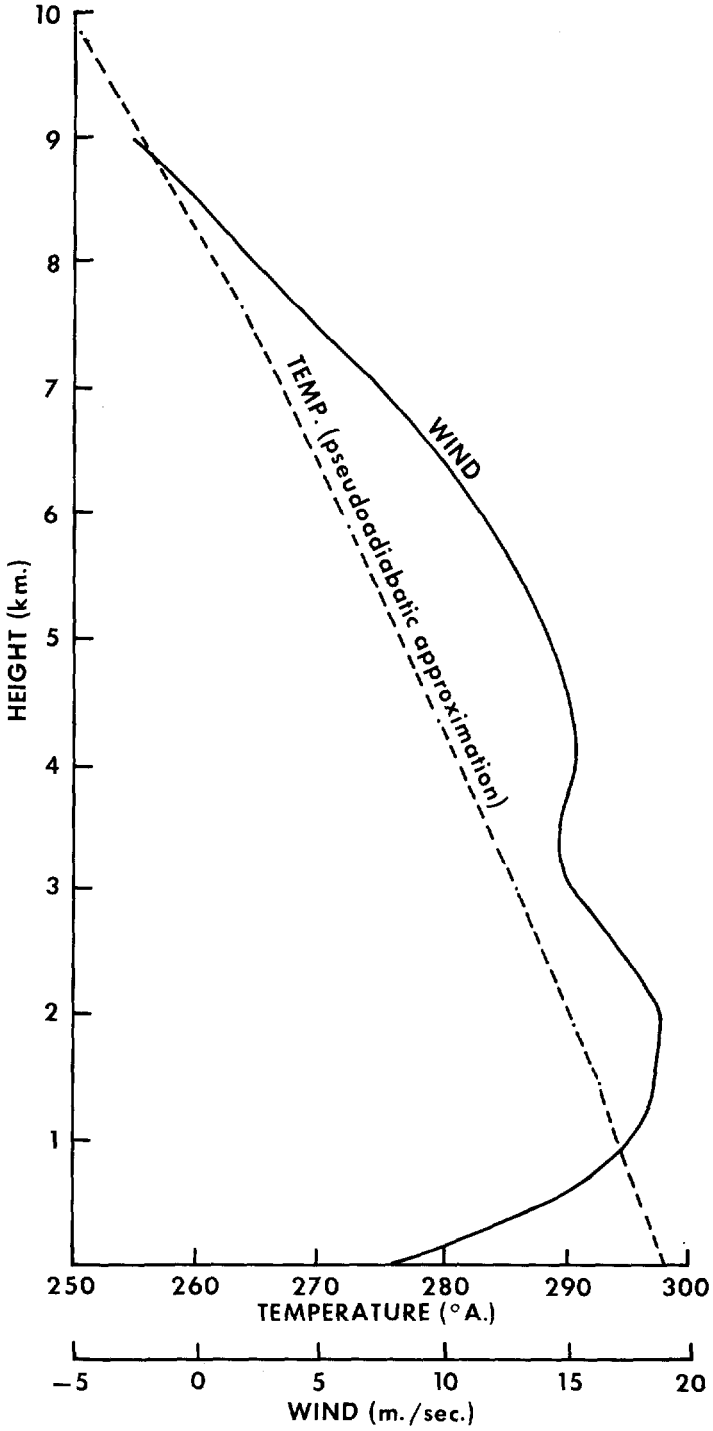

FIGURE 14.—Average wind and temperature profiles for July 11–12, 1958 (case IV).

2.5 km. to 4 km. corresponding to positive values of d^2U/dz^2. The constant values of $f(z)$ are taken as 0.30 km.$^{-2}$ from surface to 2.5 km., −0.16 km.$^{-2}$ up to 4 km., and 0.13 km. above (table 1).

The streamline and vertical velocity patterns are similar to those of the other cases. The ascending motion increases as we move toward the crest up to $x=-10$ (maximum is 32 cm. sec.$^{-1}$) after which it decreases and descends at $x=2$ km., i.e., 3 km. before the crest is reached. Also the ascending motion first increases with height then

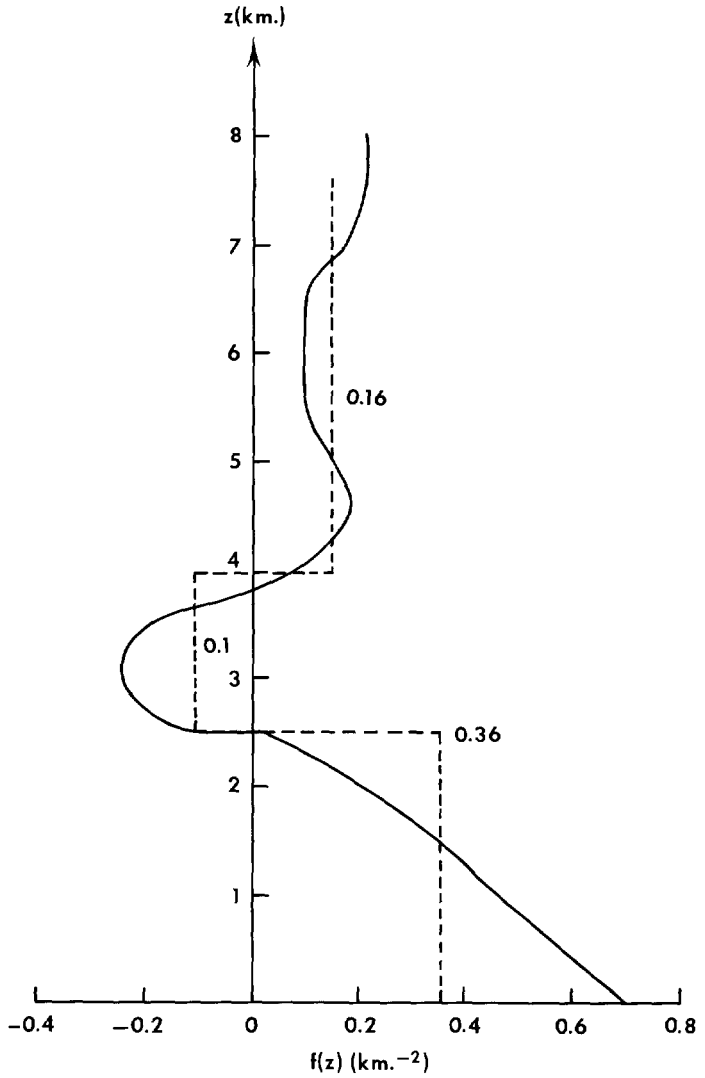

FIGURE 15.—Profile of $f(z)$ for July 11–12, 1958 (case IV).

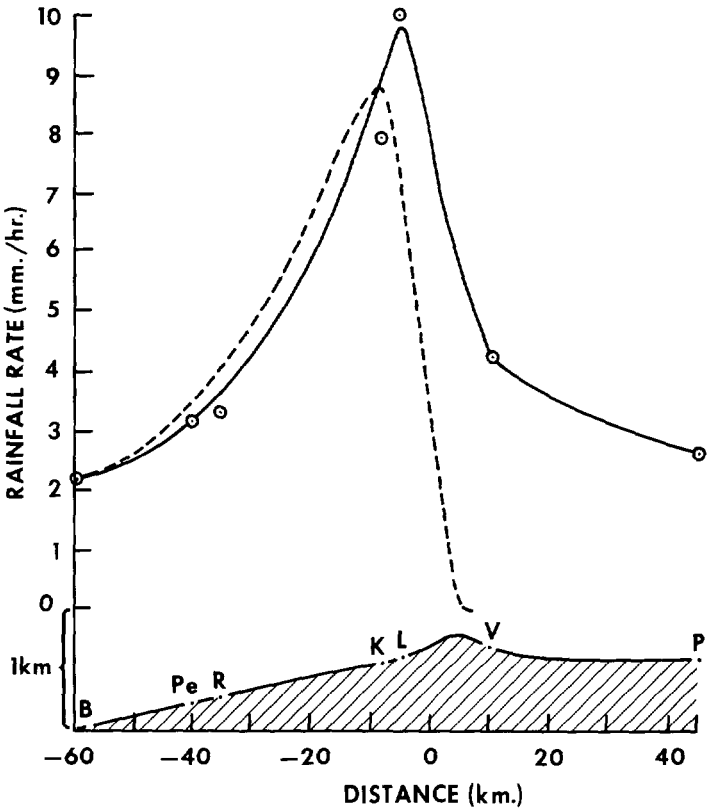

FIGURE 16.—Rainfall distribution for July 11–12, 1958 (case IV). See legend for figure 7.

decreases and becomes negative. Also up to $x=-20$ km. from the coast the motion ascends at all levels up to 7 km. Then the descending motion starts at high levels and the level of change-over from ascending to descending motion goes down gradually as one moves along the orography until the motion is entirely descending at $x=2$.

The computed orographic and the observed rainfall are in very good agreement (fig. 17). At the coast the observed rainfall is 1.8 mm./hr. and the computed orographic rainfall is 1.7 mm./hr., i.e., 94 percent of the actual. The computed orographic rainfall peak slightly exceeds the actual peak; viz., the computed orographic maximum is 9.0 mm./hr. whereas the actual maximum is 8.5 mm./hr. Also the position of the two peaks is the same. However, in this case the position and magnitude of the peak value of actual rainfall is a bit subjective as the rainfall of Lonavla (which is very near Khandala) is not available. The computed orographic rainfall at the crest of the mountain is 1 mm./hr. whereas the observed rainfall is 3 mm./hr. The spillover effect is practically nil. It appears the entire rainfall is due to orography on the windward side.

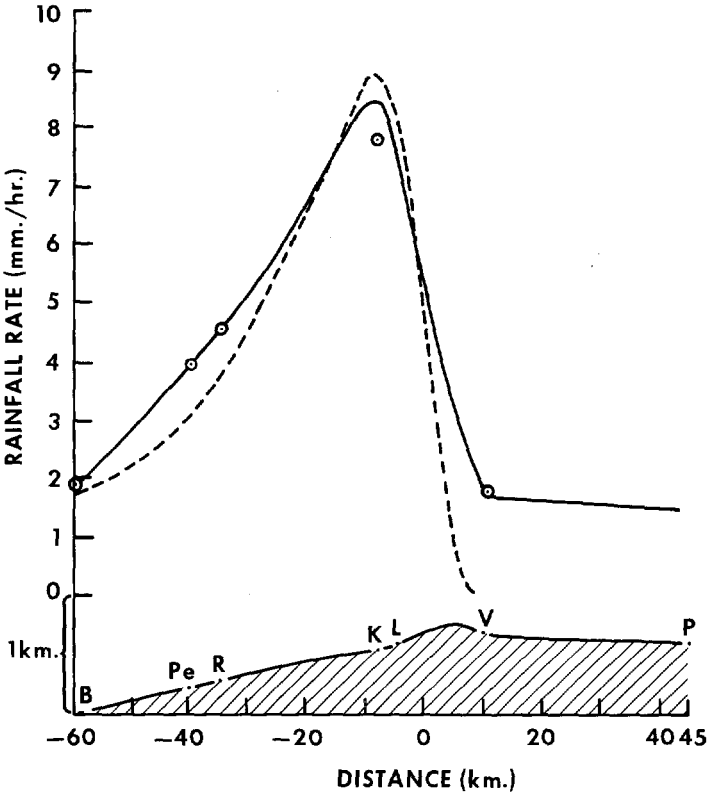

FIGURE 17.—Rainfall distribution for July 21, 1958 (case V). See legend for figure 7.

227-347 O—66——4

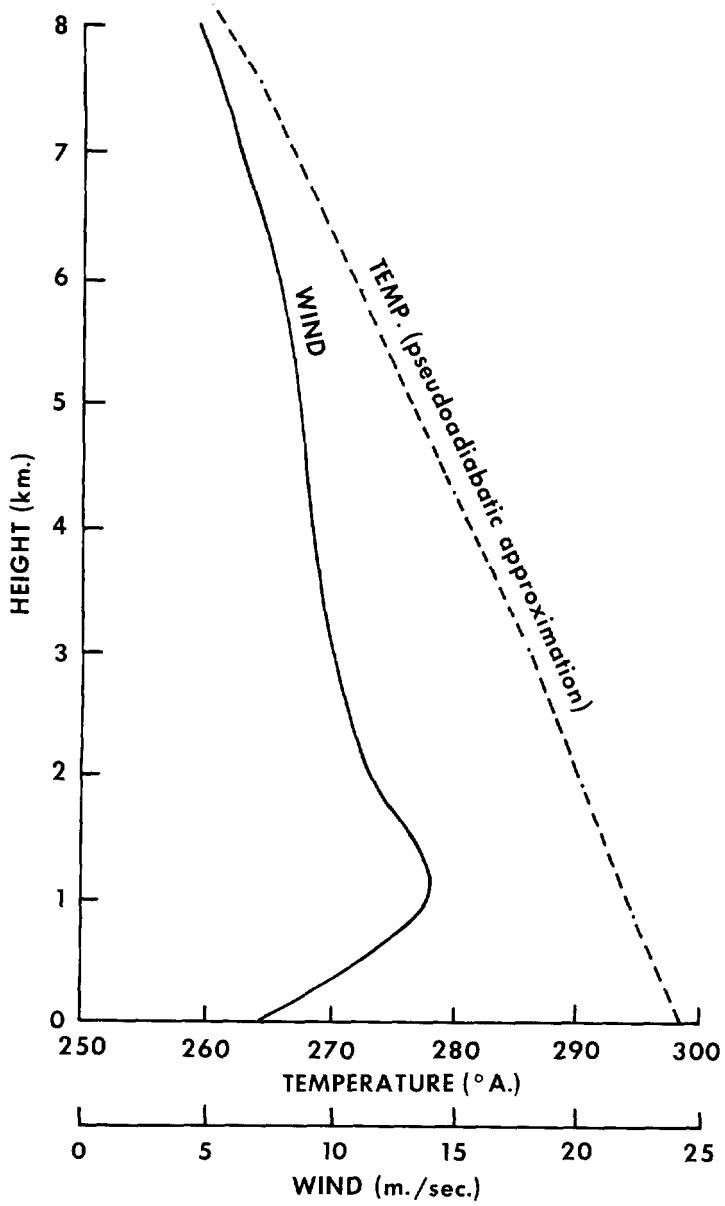

FIGURE 18.—Average wind and temperature profiles for July 2–4, 1960 (case VI).

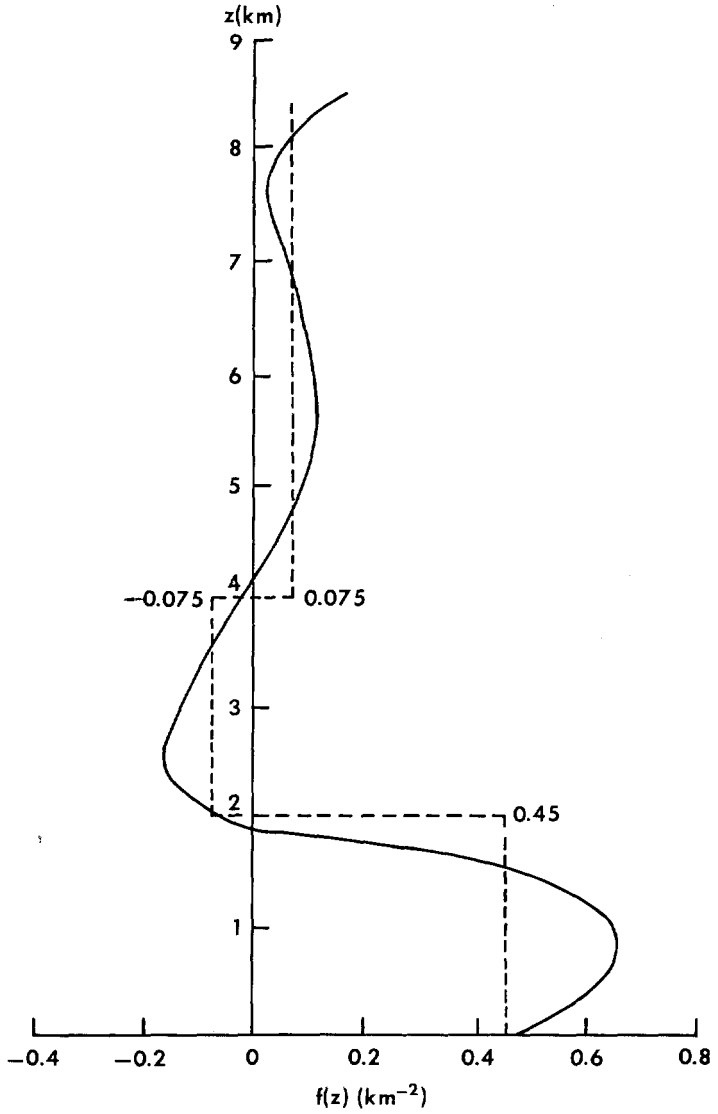

FIGURE 19.—Profile of $f(z)$ for July 2–4, 1960 (case VI).

CASE VI—JULY 2–4, 1960

The relevant average temperature and wind data are given in figure 18 for Case VI, the rainfall spell of July 2–4, 1960. The wind speed increases from 7 to 14 m./sec. at 1 km. It then decreases to 10 m./sec. at 3 km. after which it decreases slowly to 5 m./sec. at 8 km. and becomes easterly at 10.5 km. d^2U/dz^2 is negative up to 2 km., then it is positive up to 4 km., and then either negative or zero above. The surface dry bulb temperature is 300° A. and the dew point is 299° A. In the model we have taken the pseudo-adiabat through 299° A. Relative humidity is in the range 85–90 percent. Figure 19 shows $f(z)$ is negative in the layer 2 to 4 km. corresponding to positive values of d^2U/dz^2. The constant values taken for $f(z)$ are 0.45 km.$^{-2}$ up to 2 km., -0.075 km.$^{-2}$ up to 4 km., and 0.075 km.$^{-2}$ above (table 1).

The streamline and vertical velocity patterns are similar to the other cases. However, amplitude and vertical velocity seem to be slightly higher. The vertical velocity gradually increases along the orography until $x=-10$ km. after which it decreases. The maximum velocity is 31 cm./sec. Also the vertical velocity increases first with height, reaches a maximum and then decreases, and then becomes negative at higher levels. The level of change-over from ascending to descending motion goes down gradually as we proceed toward the crest and the motion is entirely descending beyond $x=-1$ km., i.e., from 4 km. before the crest is reached.

The agreement between observed rainfall and computed orographic rainfall is good (fig. 20). The observed rainfall at the coast is 2.7 mm./hr. and the computed orographic rainfall is 2.2 mm./hr., i.e., 81 percent of observed rainfall. The computed maximum orographic rainfall is 9.5 mm./hr., which is equal to the maximum observed rainfall. Also the positions of the peaks are at the same

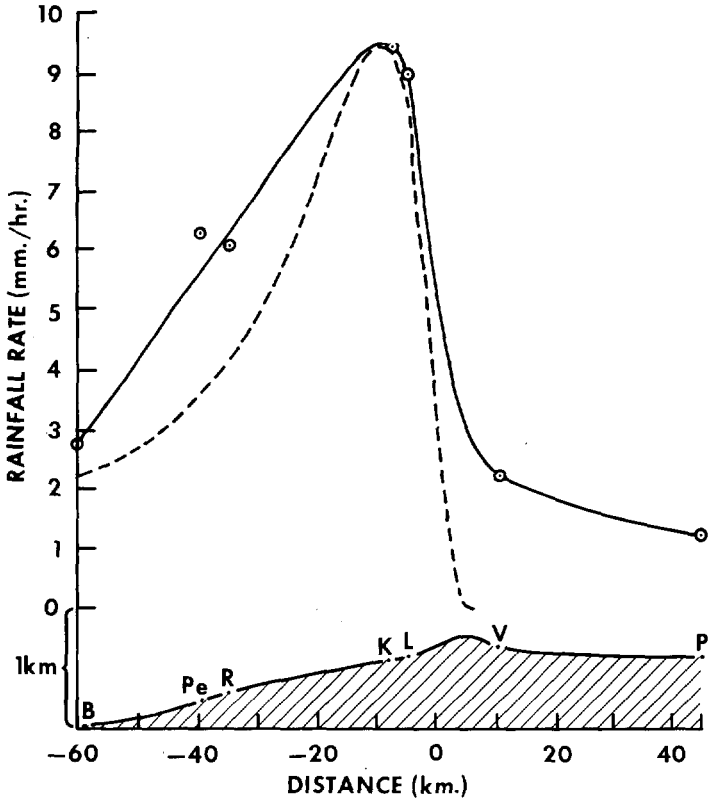

FIGURE 20.—Rainfall distribution for July 2–4, 1960 (case VI). See legend for figure 7.

point or differ at most by 2 km. The agreement even after the rainfall peaks is also good for another 8 km. The computed orographic rainfall at the crest is zero whereas the observed rainfall there is 2.8 mm./hr.

CASE VII—JULY 4–6, 1958

Case VII, the rainfall spell of July 4–6, 1958, is a very weak monsoon case. The relevant average data of wind and temperature for the spell are given in figure 21. The wind speed increases from 5 m./sec. at the surface to 13 m./sec. at 1 km. Thereafter it decreases gradually and becomes easterly just above 5 km. In this case there is no secondary maximum in wind profile. The surface dry bulb temperature is 300° A. and the dew point is 298° A. In the model, we have taken the pseudo-adiabat through 299° A. The relative humidity varies in the range 80 to 90 percent. In this case dU/dz is positive up to 1.0 km., above which it is negative and d^2U/dz^2 is negative at all levels. The $f(z)$ profile (fig. 22) is positive throughout; although $f(z)$ first decreases with height up to 2.0 km., it remains constant up to 3 km. and then increases. We have consequently considered a two-layer model in this case. The two-layer constants are 0.49 km.$^{-2}$ up to 2.25 km. and 0.16 km.$^{-2}$ above. The model will not be valid above 4 km.

Although the patterns of the streamlines and vertical velocity are similar to the other cases, the magnitude of the vertical velocity is considerably smaller and descending motion starts earlier. The ascending motion gradually increases, becomes maximum (10 cm./sec.)

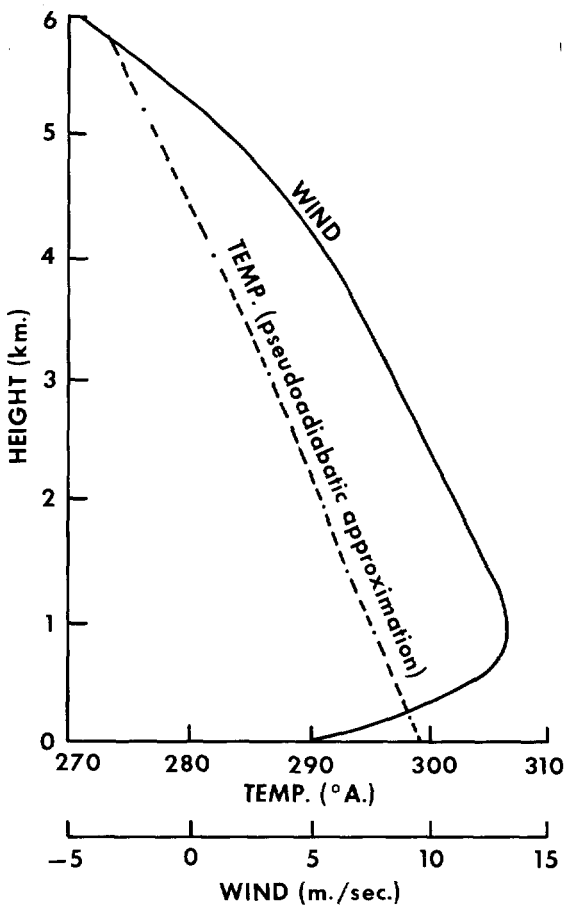

FIGURE 21.—Average wind and temperature profiles for July 4–6, 1958 (case VII).

at $x=-5$ km. and then decreases, and the motion is entirely descending beyond $x=-5$ km., i.e., from 10 km. before the crest of the mountain. The vertical velocity increases with height, becomes maximum, and then decreases and becomes negative. The level of change-over from ascending to descending motion gradually goes down as one proceeds along the orography and at and beyond $x=-5$ km. the motion is entirely descending.

The observed rainfall at the coast is 2 mm./hr. and the computed orographic rainfall is 1.2 mm./hr. or 60 percent of observed rainfall (fig. 23). The computed orographic and the observed rainfall are both small. The computed orographic rainfall, in keeping with the actual rainfall, increases very slowly along the orography. The computed maximum orographic rainfall is 2.4 mm./hr. and the observed maximum is 3.8 mm./hr., i.e., the maximum orographic rainfall is 63 percent of the observed maximum. Also the position of the computed orographic maximum is in close agreement with the position of the observed maximum. Both the peaks are at a distance of 25 km. from the crest of the mountain. The computed orographic rainfall falls off sharply beyond its peak value and the rainfall due to orography is nil at $x=-2$, i.e., 7 km. before the crest of the mountain is reached.

6. DISCUSSION

We have examined rainfall distributions both for in-

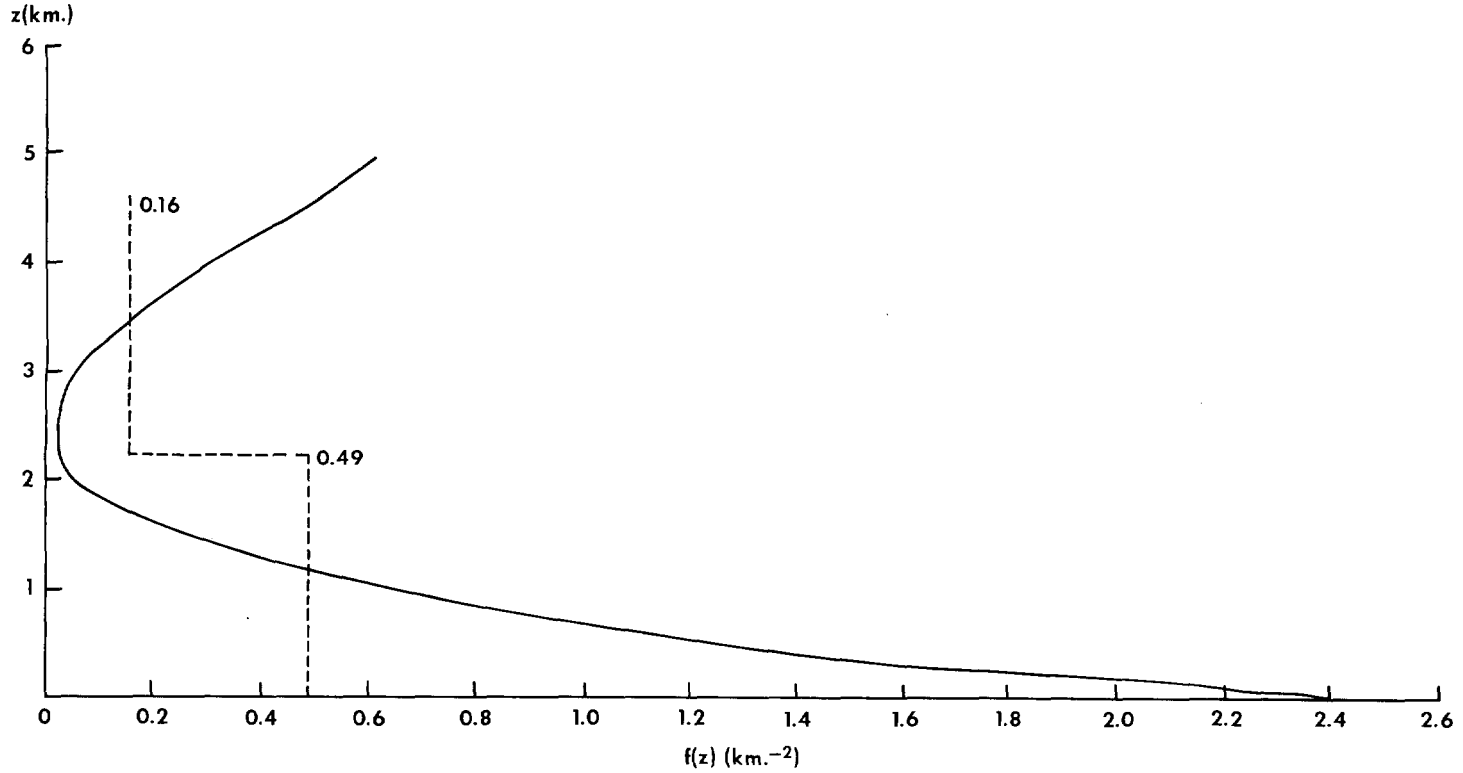

FIGURE 22.—Profile of $f(z)$ for July 4–6, 1958 (case VII).

dividual days and for spells of 2 to 4 days. Also we have examined strong monsoon as well as weak monsoon cases. In all the cases, the observed rainfall distribution on the windward side is very well explained by the dynamical model we have presented. On an average the maximum vertical velocity due to orography is of the order of 30–35 cm./sec. on a strong monsoon day, and the maximum rainfall as given by the model is of the order of 8–9 mm./hr. or 80–100 percent of the observed maximum rainfall. The maximum vertical velocity on a weak monsoon day is about 10 cm./sec. and the corresponding maximum rainfall according to our model is 2.5 mm./hr. which is of the order of 65 percent of the observed maximum rainfall. The coastal rainfall on both occasions according to our model is of the order of 1–2 mm./hr. The fact that the theoretical rainfall on the assumption of a fully saturated atmosphere does not exceed the observed rainfall even on a weak monsoon day indicates clearly that the rainfall is not entirely due to orography considered in the model. There are other factors as well.

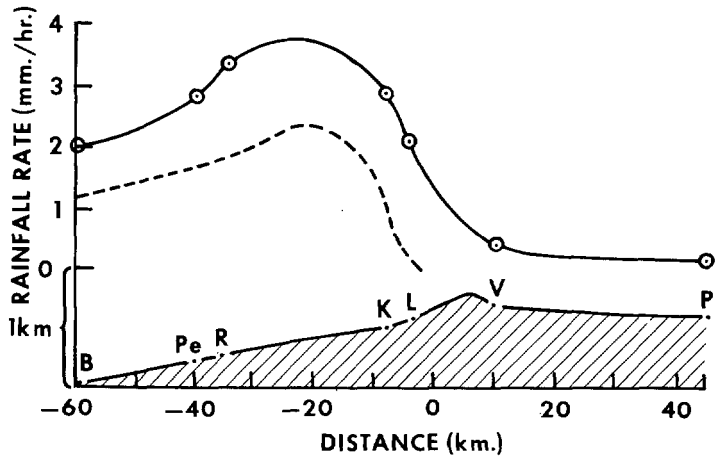

FIGURE 23.—Rainfall distribution for July 4–6, 1958 (case VII). See legend for figure 7.

However, while noting that the model suggested here is quite satisfactory, we are well aware of its limitations. And we may attribute the discrepancies between the observed rainfall and the rainfall accounted for by the model to the following reasons:

(i) We have taken a simplified smoothed profile for the terrain which in reality is not so.

(ii) We have made a simplified assumption of temperature lapse rate. We have assumed a steady streamline flow in a neutral atmosphere. The streamline flow may not be fully representative of the real atmosphere which is sometimes to some extent unstable as compared to the pseudoadiabatic lapse rate.

(iii) We have made considerable simplification in the $f(z)$ profile. We have divided the atmosphere into three layers (two for the weak monsoon case) in each of which $f(z)$ has a constant but different value.

(iv) We have made a further approximation in the evaluation of the integral in expression (12). This approximation is not strictly valid over the crest of the mountain. An exact solution of (12) would perhaps have given a

better agreement between observed and calculated rainfall in the vicinity of the crest of the mountain.

(v) We have neglected the easterly flow patterns at higher levels which might have had some effect on the flow patterns below.

(vi) Rainfall may not be entirely due to orography. Rainfall may occur as a result of lifting of saturated air from other causes as well, viz., horizontal convergence in synoptic scale and instability. The vertical velocity arising from these two causes cannot be taken into account in our model. It is quite likely that rainfall in mountain areas results from the three causes operating together.

We believe better agreement between the observed and computed rainfall may be achieved by removing the restrictions (i) to (iv) mentioned above. We propose to examine this further by approaching the problem numerically.

7. COMPARISON OF THE PRESENT MODEL WITH THE EMPIRICAL MODEL

As mentioned earlier, an empirical model for computing orographic precipitation is available [26]. In order to compare the present model with the empirical model, we have also computed orographic precipitation for our case I and case IV from the empirical model and these are represented in figures 24 and 25. All the assumptions in the empirical model are similar to those in our model except the following:

(i) In the empirical model, the flow is assumed to be horizontal at some great height, called the nodal surface, where $u=0$.

(ii) The slope of the air streamlines on a pressure coordinate, dp/dx varies linearly with pressure from the ground slope to 0 at the level $u=0$ along all the verticals.

We have used two sets of terminal velocities. In the first set rain falls at 1400 mb./hr. and snow at 190 mb./hr. In the second set the respective values are 2160 mb./hr. and 454 mb./hr. The first set is a conversion of the terminal velocities used in the present model at appropriate pressures, while the second set is a similar conversion of the terminal velocities used in [26].

It can be seen from figures 24 and 25 that there is a double hump in the rain profile from the simple empirical model. The rain profile from this model for two sets of terminal velocities is more or less similar. The first maximum in the empirical model is not in agreement with the observed distribution. The peak rainfall rate is less than the peak rate given by the model presented in this paper. Also, the peak in the empirical model shifts to the crest, whereas the peak in the observed rainfall as well as in our model is about 10–12 km. west of the crest. The total computed rainfall upwind of the crest is practically the same in both the models. The ratio of computed rainfall upwind from the present model to that computed from the empirical model is 0.93 in case I and 0.99 in case IV. The total volume including the spillover is larger in the empirical model. The corresponding ratios for total rainfall are 0.77 and 0.79. In general, the

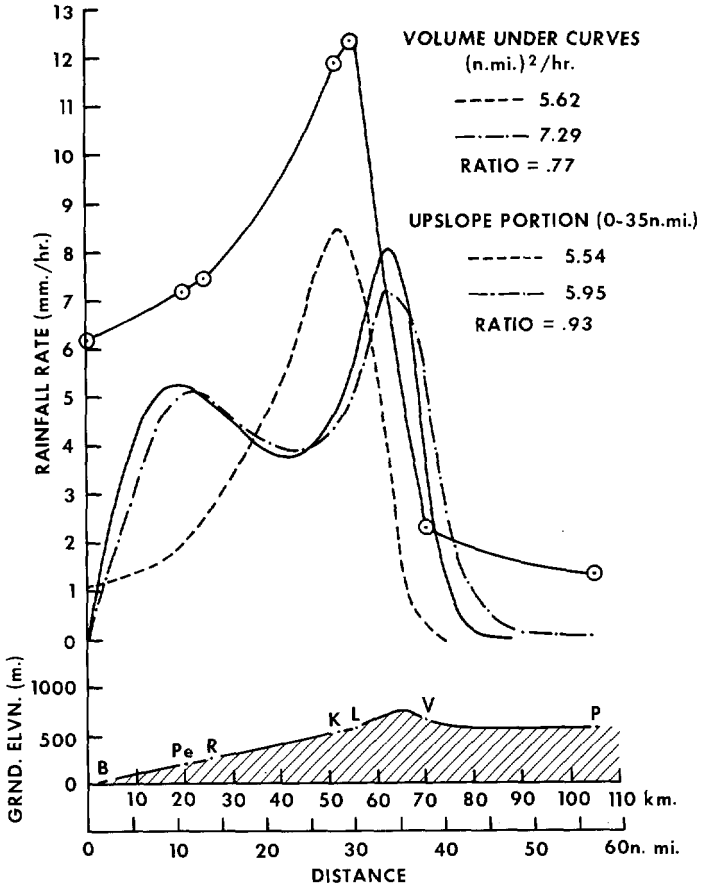

FIGURE 24.—Comparisons of observed and computed rainfall distributions for July 5, 1961 (case I): observed (heavy solid curve); theoretically computed in present study (dashed curve); computed from empirical model of [26] using terminal velocity of present study (dashed-dotted curve); computed from empirical model of [26] using terminal velocity of [26] (thin solid curve).

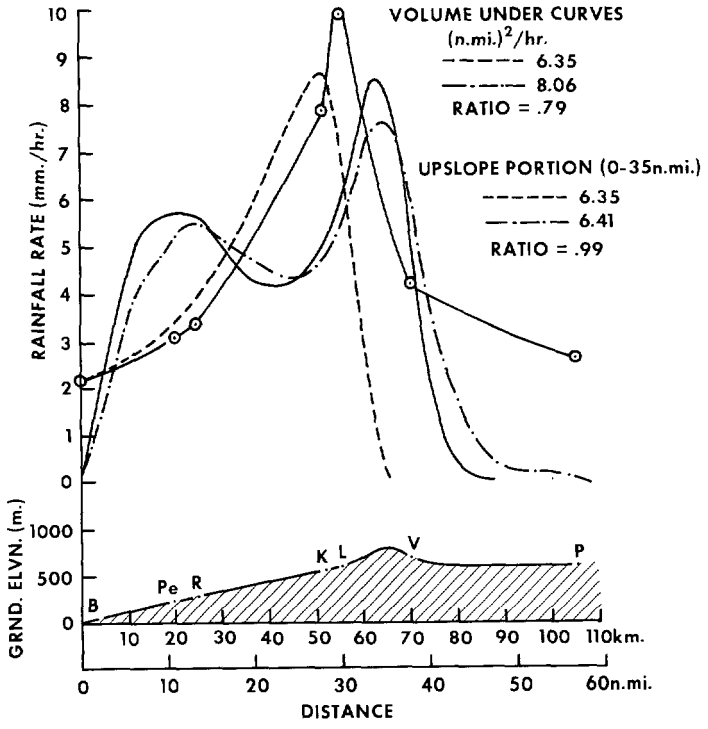

FIGURE 25.—Comparisons of observed and computed rainfall distributions for July 11–12, 1958 (case IV). See legend for figure 24.

present model explains better the rainfall distribution along the Western Ghats orography.

8. CONCLUSION

We can draw the following conclusions from this investigation.

(i) The rainfall as obtained from our dynamical model increases from coast to inland along the slope and reaches a maximum before the crest of the mountain is reached, after which it falls off sharply. This is well in agreement with the observed rainfall distribution in all the cases studied. It is seen that the normal rainfall during the monsoon also follows a similar distribution.

(ii) On a strong monsoon day, the peak of the theoretical rainfall distribution is at a distance of 10–12 km. from the crest of the mountain and on a weak monsoon day the peak is at a distance of 25 km. The positions of the peaks on both occasions are in excellent agreement with the peak of the observed rainfall.

(iii) The model accounts for, in general, 60 percent of the coastal rainfall. Apparently, rainfall at the coast is not entirely due to orography considered in our model. However, on some occasions even 80–100 percent of coastal rainfall is accounted for by the model. These might be the days when the synoptic-scale convergence and instability phenomena are at their minima.

(iv) The model accounts in most cases for 90 to 100 percent of the maximum observed rainfall. The peak in rainfall distribution is, therefore, purely an orographic effect.

(v) The spillover of rainfall due to horizontal wind does not extend beyond 10–15 km. beyond the crest of the mountain. Sometimes the model does not give any rainfall beyond the crest. Also, the computed rainfall due to spillover is negligible compared to observed rainfall on the lee side which is itself small. Apparently, the rainfall on the lee side is not due to orography considered in the model.

ACKNOWLEDGMENTS

I am thankful to Dr. P. R. Pisharoty, Director of the Institute of Tropical Meteorology, for his kind encouragement and keen interest in the course of this investigation, and to the referees for their constructive suggestions in the final preparation of the paper. Thanks are also due to Mr. N. S. Kulkarni and Mr. M. B. Pant for help in the computations.

REFERENCES

1. G. A. Corby and J. S. Sawyer, "The Air Flow over a Ridge: The Effects of the Upper Boundary and High Level Conditions," *Quarterly Journal of the Royal Meteorological Society*, vol. 84, No. 359, Jan. 1958, pp. 25–37.
2. G. A. Corby and J. S. Sawyer, "Airflow over Mountains: Indeterminacy of Solution," *Quarterly Journal of the Royal Meteorological Society*, vol. 84, No. 361, July 1958, pp. 284–285.
3. G. D. Crapper, "A Three-Dimensional Solution for Waves in the Lee of Mountains," *Journal of Fluid Mechanics*, vol. 6, 1959, pp. 51–76.
4. C. K. M. Douglas and J. Glasspoole, "Meteorological Conditions in Heavy Orographic Rainfall in the British Isles," *Quarterly Journal of the Royal Meteorological Society*, vol. 73, Jan. 1947, pp. 11–42.
5. J. R. Fulks, "Rate of Precipitation from Adiabatically Ascending Air," *Monthly Weather Review*, vol. 63, No. 10, Oct. 1935, pp. 291–294.
6. R. Gunn and G. D. Kinzer, "The Terminal Velocity of Fall for Water Droplets in Stagnant Air," *Journal of Meteorology*, vol. 6, No. 4, Aug. 1949, pp. 243–248.
7. K. L. S. Gunn and J. S. Marshall, "The Effect of Wind Shear on Falling Precipitation," *Journal of Meteorology*, vol. 12, No. 4, Aug. 1955, pp. 339–349.
8. V. N. Kelkar, "Size Distribution of Raindrops, Part 1," *Indian Journal of Meteorology and Geophysics*, vol. 10, No. 2, Apr. 1959, pp. 125–136.
9. P. M. Kuhn, "A Generalized Study of Precipitation Forecasting. Part 2: A Graphical Computation of Precipitation," *Monthly Weather Review*, vol. 81, No. 8, Aug. 1953, pp. 222–232.
10. M. P. Langleben, "The Terminal Velocity of Snowflakes," *Quarterly Journal of the Royal Meteorological Society*, vol .80, No. 344, Apr. 1954, pp. 174–181.
11. R. J. List (compiler), *Smithsonian Meteorological Tables*, 6th ed., Smithsonian Institution, Publication 4014, 1951, (see pp. 327 and 396).
12. F. H. Ludlam, "Artificial Snowfall from Mountain Clouds," *Tellus*, vol. 7, No. 3, Aug. 1955, pp. 277–290.
13. F. H. Ludlam, "The Structure of Rainclouds," *Weather*, vol. 11, No. 6, June 1956, pp. 187–196.
14. J. S. Marshall, "Precipitation Trajectories and Patterns," *Journal of Meteorology*, vol. 10, No. 1, Feb. 1953, pp. 25–29.
15. B. J. Mason and J. B. Andrews, "Drop-Size Distributions from Various Types of Rain," *Quarterly Journal of the Royal Meteorological Society*, vol. 86, No. 369, July 1960, pp. 346–353.
16. E. Palm, "Airflow over Mountains: Indeterminacy of Solution," *Quarterly Journal of the Royal Meteorological Society*, vol. 84, No. 362, Oct. 1958, pp. 464–465.
17. E. Palm and A. Foldvik, "Contribution to the Theory of Two-Dimensional Mountain Waves," *Geofysiske Publikasjoner*, vol. 21, No. 6, Mar. 1960, 30 pp.
18. P. Queney et al., "The Airflow over Mountains: Report of a Working Group of the Commission for Aerology," *Technical Note* No. 34, World Meteorological Organization, Geneva, 1960, 135 pp.
19. R. P. Sarker, "A Theoretical Study of Mountain Waves on Western Ghats," *Indian Journal of Meteorology and Geophysics*, vol. 16, No. 4, 1965, pp. 565–584.
20. J. S. Sawyer, "The Physical and Dynamical Problems of Orographic Rain," *Weather*, vol. 11, No. 12, Dec. 1956, pp. 375–381.
21. J. S. Sawyer, "Numerical Calculation of the Displacements of a Stratified Airstream Crossing a Ridge of Small Height," *Quarterly Journal of the Royal Meteorological Society*, vol. 86, No. 369, July 1960, pp. 326–345.
22. R. S. Scorer, "Theory of Waves in the Lee of Mountains," *Quarterly Journal of the Royal Meteorological Society*, vol. 75, Jan. 1949, pp. 41–56.
23. R. S. Scorer, "Theory of Airflow over Mountains: II—The Flow over a Ridge," *Quarterly Journal of the Royal Meteorological Society*, vol. 79, No. 339, Jan. 1953, pp. 70–83.
24. A. K. Showalter, "Rates of Precipitation from Pseudo-Adiabatically Ascending Air," *Monthly Weather Review*, vol. 72, No. 1, Jan. 1944, p. 1.
25. J. C. Thompson and G. O. Collins, "A Generalized Study of Precipitation Forecasting. Part 1: Computation of Precipitation from the Fields of Moisture and Wind," *Monthly Weather Review*, vol. 81, No. 4, Apr. 1953, pp. 91–100.
26. U.S. Weather Bureau, "Interim Report—Probable Maximum Precipitation in California," *Hydrometeorological Report*, No. 36, Washington, D.C., Oct. 1963, 202 pp.

[*Received February 16, 1966; revised June 21, 1966*]